Simulations of Linear Block Copolymers in Liquid Chromatography at the Critical Condition

A THESIS
SUBMITTED TO THE FACULTY OF THE GRADUATE SCHOOL
OF THE UNIVERSITY OF MINNESOTA
BY

Kimberly Nicole Struksheats

IN PARTIAL FULFILLMENT OF THE REQUIREMENTS
FOR THE DEGREE OF
DOCTOR OF PHILOSOPHY

J. Ilja Siepmann

August, 2017

Acknowledgements

First and foremost, I would like to thank my husband Julian Struksheats for his endless support during my undergraduate and graduate student careers. Words are simply insufficient to express the amount of gratitude I have for him.

I would like to thank my parents, Chris and Dee Struk, for their encouragement and understanding as I've taken this path that has lead me to move to ever more distant locations from them. Our phone calls made the distance between Minneapolis and Tallahassee seem a lot shorter than it is. Thank you to my siblings Daniel, Rachel, and Zoe Struk for providing emotional support in a way that only siblings can.

A special thank you to fellow graduate students Elyse Krautkramer, Amanda Oehrlein, and Katie Youmans for always providing me the opportunity to vent when I needed it. Nothing can replace the camaraderie we have gained through this shared experience.

I would also like to thank Bekah and Jeff Metzdorff of Mill City Running for forming an amazing race team which helped me run off the stress of graduate school. Their enthusiasm always helped me recover from a rough day.

Thank you to to my adviser Ilja Siepmann for his guidance during my graduate career and assisting me with getting an internship position at Lawrence Livermore National Laboratory during my fourth year.

Thank you to my research group members for their suggestions to help improve my work. In particular, I would like to thank Becky Lindsey for helping me learn the ropes of simulation and statistical mechanics as I transitioned from experimental to simulation work.

Additionally, I would like to thank Will Kuo, Sorin Bastea, and Rick Gee of Lawrence Livermore National Laboratory for the opportunity to intern with them and their patience and guidance as they taught me about new methods and areas of

simulation and working at a national lab. Thank you to Mark Schure of Kroungold Analytical for providing very helpful guidance on writing scientific manuscripts.

Finally, funding from the National Science Foundation, Dow, and the University of Minnesota Materials Research Science and Engineering Center are gratefully acknowledged. Computing resources from the Minnesota Supercomputing Institute and Livermore Computing were instrumental in allowing me to perform this work.

Abstract

Liquid chromatography at the critical condition (LCCC) is often used for analysis of block copolymers where solvent conditions are chosen such that the molecular weight dependence of one of the blocks upon retention is negligible. In this work, Gibbs ensemble Monte Carlo simulations are used to determine partition constants of block copolymer chains moving between mobile and spherical- or cylindrical-shaped stationary phases. With these simulations, we explore the limitations of using LCCC to characterize the molecular weight distribution of block copolymers with various sequences. Thermodynamic properties of transfer are shown to vary with sequence and are dependent on temperature. Informed by the monomer-level adsorption analysis, new calibration equations relating partition constant and sequence are proposed.

Contents

List of Tables

List of Figures

Chapter 1

Introduction

Polymers play many roles in modern life from simple applications like poly(ethylene terephthalate) used in beverage bottles to highly technical applications such as drug delivery, electronic devices, and medical devices where designer copolymers of varying architectures and compositions are required [1, 2, 3]. The molecular weight distribution (MWD) of a polymer sample is integral to product performance in these applications. Liquid chromatography techniques, in particular size exclusion chromatography (SEC), are commonly used to characterize the MWD of a polymer sample; however, this technique is unable to give accurate data for copolymer systems [4, 5]. Given the rise of copolymer synthesis, a new method, liquid chromatography at the critical condition (LCCC), was devised to help accurately characterize the MWD these polymers [6]. Several recent experimental studies contest the validity of this technique [7, 8, 9, 10, 11]. The main focus of this work is to test the assumptions and validity of the LCCC methodology using the molecular-level insight gained from Monte Carlo simulations.

1.1 Polymer Chromatography

Unlike small molecules, a polymer sample may be composed of molecules with a wide range of molecular weights. Even polymer chains prepared in just one synthesis experiment have varying lengths; hence, producing a "molecular weight distribution" (MWD) that varies based on polymerization type and reaction conditions. The MWD affects the physical properties of the final product and thus is important to

properly characterize. When describing a polymer sample, two average chain length definitions are commonly used: the number-average molecular weight, M_{n}, and the weight-average molecular weight, M_{w}, which are defined below [2]:

$$M_{\mathrm{n}} = \frac{\sum_i n_i M_i}{\sum_i n_i} \tag{1.1}$$

$$M_{\mathrm{w}} = \frac{\sum_i n_i M_i^2}{\sum_i n_i M_i} \tag{1.2}$$

where n_i is the number of chains with degree of polymerization i, and M_i is the molecular weight of the i-mer. The ratio of M_{w} to M_{n} yields the dispersity, Đ, which describes the spread of the chain lengths in the sample. A dispersity value of unity means that all chains in the sample are the same length while larger values indicate broader MWDs.

These average molecular weights are straightforward to determine when one knows the distribution of chain lengths in a polymer sample; however, polymer syntheses do not immediately yield this information at the end of the reaction based on the amount of reagents consumed, reaction time, or by the appearance of the product. Instead, chromatographic techniques are commonly used to separate the chains to determine the MWD [4]. The remainder of this section provides a brief introduction into column chromatography and then chromatographic techniques specifically designed for characterizing polymers.

1.1.1 Liquid Chromatography

Column chromatography dates back to the early 1900's and is widely used due to its relative ease to separate compounds for preparative or analytical needs [4, 12, 13, 14]. While there are many varieties of column chromatography, let us initially focus on liquid chromatography (LC). In LC, a column is connected to a solvent source and a sample injector on one end and a detector, or multiple detectors, are attached to the other end. The solutes are separated according to the strength of their interactions with the stationary phase, repulsive or attractive interactions with the surface of the column packing material; and with the mobile phase, the solvent. The output from a typical LC experiment can look similar to Fig. 1.1, where each peak contains one or multiple analytes. Analytes that reside primarily in the mobile phase elute

before those that reside more in the stationary phase. Ideally, each peak would be very narrow and Gaussian-shaped, and all peaks would be baseline resolved; however, peak broadening and tailing, along with similar elution times for different species lead to non-Gaussian peak shapes. Peak broadening is influenced by many factors such as sample concentration, mobile phase rate, and column packing particle size.

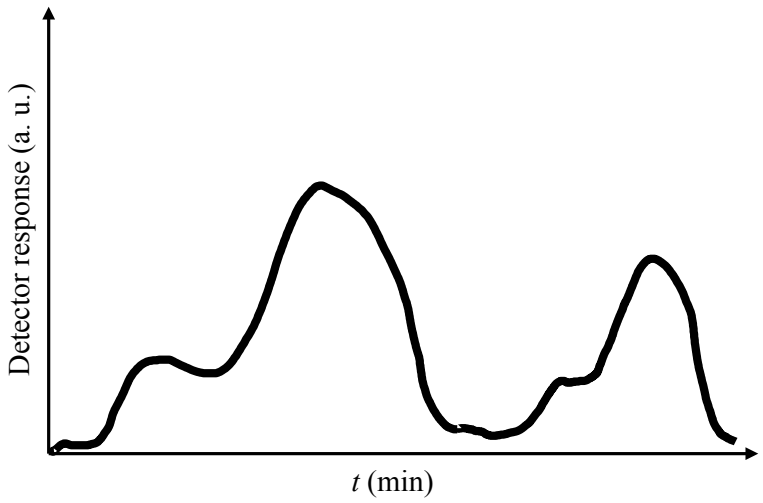

Figure 1.1: Sketch of a LC chromatogram.

Despite the flow present in LC, the solute transfer between the two phases is understood to be an equilibrium process [14, 15]. This can be written out for an analyte A moving between mobile (mob) and stationary (stat) phases as:

$$\mathrm{A_{mob}} \leftrightharpoons \mathrm{A_{stat}} \tag{1.3}$$

The partition coefficient, K, is defined as the ratio of analyte concentrations in the two phases:

$$K_{\mathrm{A}} = \frac{n_{\mathrm{A,stat}}/V_{\mathrm{stat}}}{n_{\mathrm{A,mob}}/V_{\mathrm{mob}}} = \frac{c_{\mathrm{A,mob}}}{c_{\mathrm{A,stat}}} \tag{1.4}$$

where n is the number of A molecules in each phase, V is the volume of each phase, and c is the concentration of A in each phase. Unfortunately, K can not be directly measured in a LC experiment, but a related factor, the retention time, t_{ret}, is measured. The retention time is the sum of the time the analyte spends in the stationary phase, t_{stat} and the time it takes for the mobile phase to reach the detector, t_{mob}.

$$t_{\mathrm{ret}} = t_{\mathrm{stat}} + t_{\mathrm{mob}} \tag{1.5}$$

With a known length of the column, L, the average analyte linear velocity, v, and average mobile-phase molecule velocity, u, can be determined from:

$$v = \frac{L}{t_{\text{ret}}} \tag{1.6}$$

and

$$u = \frac{L}{t_{\text{mob}}} \tag{1.7}$$

The analyte velocity can be described as a fraction of the mobile-phase molecules:

$$v = u \times (\text{fraction of time analyte spends in mobile phase}) \tag{1.8}$$

which can also be defined as

$$v = u \times \frac{n_{\text{A,mob}}}{n_{\text{A,mob}} + n_{\text{A,stat}}} \tag{1.9}$$

Introducing the volume of each phase allows us to re-write Eqn. 1.9 as:

$$v = u \times \frac{c_{\text{mob}} V_{\text{mob}}}{c_{\text{mob}} V_{\text{mob}} + c_{\text{stat}} V_{\text{stat}}} = u \times \frac{1}{1 + c_{\text{stat}} V_{\text{stat}} / c_{\text{mob}} V_{\text{mob}}} \tag{1.10}$$

Substitution of Eqn. 1.4 into Eqn. 1.10 yields:

$$v = u \times \frac{1}{1 + K_{\text{A}} V_{\text{stat}} / V_{\text{mob}}} \tag{1.11}$$

The retention factor, k, is introduced to compare migration rates of multiple analytes as it does not depend on the mobile-phase flow rate through the column, allowing for easier comparison between multiple experiments performed on the same column with the same solvent system. It is defined as

$$k_{\text{A}} = \frac{K_{\text{A}} V_{\text{stat}}}{V_{\text{mob}}} \tag{1.12}$$

Substituting Eqn. 1.12 into Eqn. 1.11 yields

$$v = u \times \frac{1}{1 + k_{\text{A}}} \tag{1.13}$$

Recalling the definitions of v and u and using these in Eqn. 1.13 gives the relationship between the retention and time and k_{A}

$$\frac{L}{t_{\text{ret}}} = \frac{L}{t_{\text{mob}}} \times \frac{1}{1 + k_{\text{A}}} \tag{1.14}$$

This can be rearranged to

$$k_{\mathrm{A}} = \frac{t_{\mathrm{ret}} - t_{\mathrm{mob}}}{t_{\mathrm{mob}}} \tag{1.15}$$

One advantage of using Gibbs ensemble Monte Carlo simulations, is that one may easily obtain the analyte density in each phase. The ratio of these two densities can be used to determine the partition coefficient, K, which is then used to calculate the Gibbs free energies of transfer, $\Delta G_{\mathrm{trans}}$, by using Eqn. 1.16 [15, 16]:

$$\Delta G_{\mathrm{trans}} = -RT \ln K \tag{1.16}$$

where R is the universal gas constant and T is the absolute temperature.

1.1.2 Size Exclusion Chromatography

A variant of LC, gel permeation chromatography, was first used for polymers in 1964 to characterize the molecular weight of polystyrene samples [17]. As time progressed and the method became better understood, the preferred nomenclature changed from "gel permeation chromatography" to "size exclusion chromatography" (SEC) [1, 2]. This method is still one of the most popular methods for separating and characterizing polymers [18]. Like in "traditional" LC, there is a liquid mobile phase that carries the solute through the column. Furthermore, the column is packed with porous beads, as illustrated in Fig. 1.2. While small chains may still sample many degrees of conformational freedom when within a pore, larger chains are able to sample only a few degrees of configurational freedom when within a pore and are excluded from very small pores. This entropic effect results in higher retention of small chains compared to long chains, as illustrated in Fig. 1.2 (B). Long polymer chains have shorter elution times than small chains as illustrated in Fig. 1.2 (C) and (D).

The polymer partition coefficient is influenced by the solvent as chain separation is actually dependent on the hydrodynamic volume of the particular polymer in the chosen solvent, rather than directly on the degree of polymerization. Different scaling relationships between the degree of polymerization, N, and the hydrodynamic volume, V_{h}, based on the quality of the solvent for a particular polymer have been determined [2]. This requires the assumption that V_{h} is proportional to the radius of

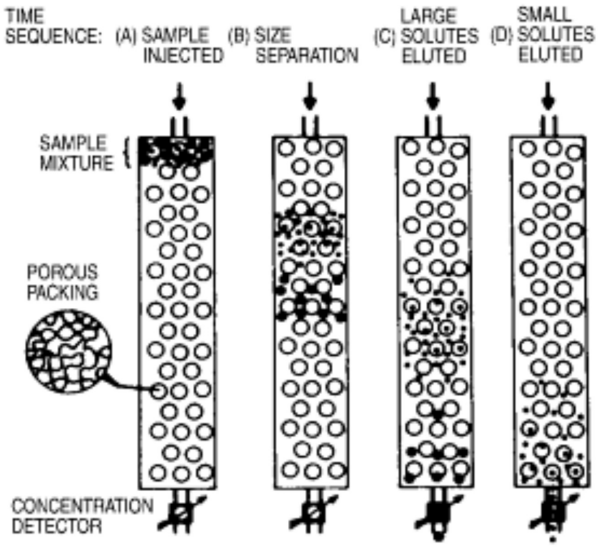

Figure 1.2: Illustration of a SEC retention process. Image taken from [1].

gyration, R_{g}, as shown:

$$V_{\mathrm{h}} \propto \frac{3}{4}\pi R_{\mathrm{g}}^3 \tag{1.17}$$

From here, R_{g} is related to N through the Flory exponent, ν:

$$R_{\mathrm{g}} \propto N^{\nu} \tag{1.18}$$

The value of the exponent varies from 1/3 for spheres which are similar to polymers in poor solvents, 1/2 for flexible coils in theta solvents, 3/5 for flexible chains in good solvents, to unity for rigid rods.

To account for the different scaling relationships, solvent and temperature effects, and proportionality factors, the conversion from elution time to molecular weights is usually done by comparing to calibration curves run under the same conditions. Standards for common polymers such as polystyrene are available over a wide range of molecular weights; however, standards for polymers made from novel monomers are generally unavailable. In these cases, polystyrene standards are still frequently used for the calibration curve, but since each solvent solvates each polymer differently, polystyrene standards often yields inaccurate MWDs.

1.1.3 Liquid Chromatography at the Critical Condition

More recent developments in polymer synthesis have yielded polymer chains that are composed of multiple monomers in a single polymer chain, known as copolymers, that exhibit unique morphologies and thus are the subject of much interest [3, 19, 20]. As alluded to previously, different polymers have different scaling relationships between hydrodynamic volume and degree of polymerization under the same conditions. As such, it is impossible to use SEC to determine an accurate MWD for a copolymer sample and new variations of SEC have been developed to better characterize the MWD of copolymers.

The SEC variant studied in this work is known by "liquid chromatography at the critical condition" (LCCC) which was first described in 1986 [21, 22]. The "critical condition" refers to the solvent, column, and temperature combination that results in co-elution of homopolymers, independent of molecular weight. A sketch of the relationship between molecular weight (M) and retention time for SEC and LCCC is given in Fig. 1.3. Calibration curves similar to Fig. 1.3 are prepared when using SEC to determine the molecular weight of a synthesized polymer. The x-axis is either time or retention volume while the y-axis is typically log M. Experimental practice uses log M as it yields an approximately linear relationship over two orders of magnitude in M in SEC [2]. Poor separation is responsible for the nonlinear relationships at either end of the time scale. All chains too large to fit into any pores elute together at a short elution time corresponding to the time required to flow through the voids between packing beads. Polymer chains small enough to enter all pores elute with the solvent are represented in the nonlinear portion at long retention time. In LCCC, all chain lengths co-elute at the same time so a narrow peak is observed.

In SEC, separation is primarily directed by entropic effects: shorter chains have many more accessible configurational degrees of freedom within a pore than longer chains, hence, shorter chains are more retained and have higher partition coefficients. Adding an additional repeat unit to the chain decreases the number of accessible configurational degrees of freedom as a longer chain is excluded from more pores. In LCCC, this incremental entropic penalty is balanced with an enthalpic gain that occurs from an additional repeat unit adsorbing onto the pore surface. This results in minimal chromatographic separation for chains of different molecular weights. As all chain lengths of one monomer type co-elute, this monomer type is at the "critical

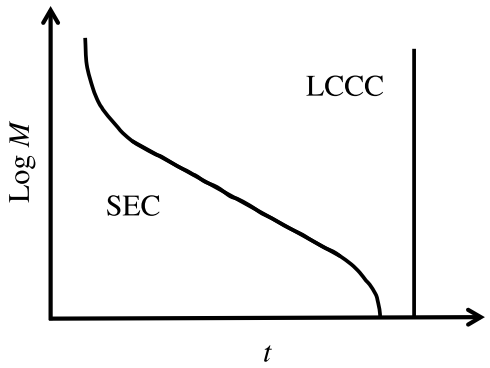

Figure 1.3: Sketch of the relationship between molecular weight, M, and elution time, t, for SEC and LCCC.

condition" and thus appears to be "chromatographically invisible." While it may seem odd to choose operating conditions such that one has no separation, this approach becomes more useful when multiple monomers are present in the chain. When one of the monomers of a copolymer is at the critical condition, separation is supposed to be purely dependent on the hydrodynamic volume composed of other monomer types. This process is repeated for both monomer types present in a two-component polymer to yield the degree of polymerization for each component and the total MWD for the polymer sample.

There has been much debate over whether LCCC yields accurate MWD data for block copolymers based on both experimental [7, 8, 9, 10, 11] and simulation [23, 24, 25, 26, 27, 28, 29, 30] data. The goal of the LCCC component of this work is to assess the LCCC method by using computer simulation and demonstrate the limitations of this technique with model linear polymers which is discussed in Chapter 3 of this work.

Chapter 2

Theory and Methods

As mentioned in Chapter 1, scientific insight can be limited by the resolution of characterization techniques and many experiments can be too dangerous or create too much hazardous waste to perform. This chapter focuses on developing the background for the primary simulation techniques utilized in this body of work. First, there is a brief overview of statistical mechanics which is followed by a discussion of the Monte Carlo simulation approach and advanced algorithms which enable efficient polymer simulations.

2.1 Statistical Mechanics

Chemists tend to take either a macroscopic or a microscopic view of a system of interest. From the macroscopic perspective, solutions are described by properties such as temperature, volume, and concentration, but molecular scale information is generally unknown. From the microscopic perspective, one knows the locations of individual atoms and the electron distributions around them. Statistical mechanics serves as the bridge from molecular configurations to macroscale thermodynamic properties.

When using the microscopic perspective, one finds that the possible number of states for a macroscopic-sized system (roughly 10^{24} molecules) is quite large. The term "ensemble" is used to describe a collection of a very large number of systems that satisfy the same set of macroscopic constraints, but represent different microscopic states [31, 32]. To connect the ensemble used in statistical mechanics and macroscopic properties, we first begin with the three postulates of statistical mechanics:

1. An isolated system can be found with equal probability in any of its accessible quantum (or classical) states. This is known as the principle of equal *a priori* probabilities.

2. Ensemble averages are equivalent to time averages, provided that the time average is taken over a period of time greater than the number of subsystems in the ensemble times the relaxation time of the system. This is known as the ergodic hypothesis.

3. The weighted average value of a mechanical property taken over all accessible microscopic states corresponds to a parallel thermodynamic property.

This work uses the Gibbs-NVT ensemble which has constant number of particles, N, volume, V, and absolute temperature, T. This is a multi-box variant of the canonical ensemble which allows for simultaneous sampling of multiple phases that are in chemical equilibrium with each other. To begin the discussion on specific topics within statistical mechanics pertinent to this work, we will initially focus on the canonical ensemble which is used for single box systems with known N, V, and T, and discuss the Gibbs-NVT ensemble in Section 2.4.

The partition function of the canonical ensemble, $Q(N, V, T)$, is

$$Q(N, V, T) = \sum_j e^{E_j/k_\mathrm{B}T} \tag{2.1}$$

and the probability that the system is in energy state E_j is given by

$$P_j(N, V, T) = \frac{e^{E_j/k_\mathrm{B}T}}{Q(N, V, T)} \tag{2.2}$$

where E_j is the energy of quantum state j and k_B is the Boltzmann constant. This summation is for all accessible states of a system. Using Eq. 2.2 and the third postulate, one can compute an average mechanical property, $\bar{M}$ of the system using:

$$\bar{M} = \sum_j M_j P_j \tag{2.3}$$

The quantized canonical partition function may be extended to a continuous version for classical mechanics by assuming that energy is a continuous function of atomic positions and momenta and using the classical Hamiltonian $H(\mathbf{q}^N, \mathbf{p}^N)$ where

$\mathbf{q}^N = q_1, q_2, \cdots, q_N$ is the set of all positions and $\mathbf{p}^N = p_1, p_2, \cdots, p_N$ is the set of all momenta. We can convert the summation in Eqn. 2.1 to a multidimensional integral over the set of $3N$ coordinates, $\mathbf{q}^N$, and $3N$ momenta, $\mathbf{p}^N$ to yield

$$Q_{\text{class}} = \frac{c}{N!} \int_{-\infty}^{+\infty} \cdots \int_V e^{-H(\mathbf{q}^N, \mathbf{p}^N)/k_\text{B}T} \text{d}\mathbf{p}^N \text{d}\mathbf{q}^N \tag{2.4}$$

where c is a constant that ensures Q and Q_{class} are equal and $1/N!$ accounts for indistinguishable particles.

Now, let us assume that the Hamiltonian can be separated into terms representing kinetic and potential energy and that we only have translational degrees of freedom. This yields

$$H(\mathbf{q}^N, \mathbf{p}^N) = \frac{1}{2m} \sum_{j=1}^{N} (p_{xj}^2 + p_{yj}^2 + p_{zj}^2) + U(\mathbf{q}^N) \tag{2.5}$$

We can substitute Eqn. 2.5 into Eqn. 2.4 and integrate over the momenta which yields

$$Q_{\text{class}} = \frac{1}{N!} \left(\frac{2\pi m k_\text{B} T}{h^2} \right)^{3N/2} Z_N \tag{2.6}$$

where

$$Z_N = \int \cdots \int e^{-U(\mathbf{q}^N)/k_\text{B}T} \text{d}\mathbf{q}^N \tag{2.7}$$

is called the configurational integral, and the exponential term is the Boltzmann weight. By introducing the thermal de Broglie wavelength, Λ, defined as

$$\Lambda = \left(\frac{h^2}{2\pi m k_\text{B} T} \right)^{1/2} \tag{2.8}$$

We can substitute Λ into Eqn. 2.6 which results in

$$Q_{\text{class}} = \frac{Z_N}{N! \Lambda^{3N}} \tag{2.9}$$

Recalling the third postulate, we can use Eqn. 2.9 to compute the average of a thermodynamic property, $\langle M \rangle$, with

$$\langle M \rangle = \frac{1}{Q_{\text{class}}} \int \cdots \int M(\mathbf{q}^N, \mathbf{p}^N) e^{-U(\mathbf{q}^N, \mathbf{p}^N)/k_\text{B}T} \text{d}\mathbf{p}^N \text{d}\mathbf{q}^N \tag{2.10}$$

which simplifies to

$$\langle M \rangle = \frac{1}{Z_N} \int \cdots \int M(\mathbf{q}^N) e^{-U(\mathbf{q}^N)/k_\mathrm{B}T} \mathrm{d}\mathbf{q}^N \tag{2.11}$$

when examining properties that only depend on the particle positions.

To determine thermal properties, we need to determine the entropy of the system, which is given by

$$S(N,V,T) = -k_\mathrm{B} \sum_j P_j \ln P_j = -\frac{k_\mathrm{B}}{Q(N,V,T)} \sum_j e^{E_j/k_\mathrm{B}T} \left(-\frac{E_j}{k_\mathrm{B}T} - \ln Q(N,V,T) \right) \tag{2.12}$$

and the average energy of the system, $\bar{E}$. Since E is a mechanical property we may use Eq. 2.3

$$\bar{E} = \sum_j E_j P_j = \frac{\sum_j E_j e^{E_j/k_\mathrm{B}T}}{Q(N,V,T)} \tag{2.13}$$

From thermodynamics we have the relation

$$S = \frac{E}{T} - \frac{A}{T} \tag{2.14}$$

where A is the Helmholtz free energy. We can combine Equations 2.12, 2.13, and 2.14 to yield

$$S = \frac{\bar{E}}{T} + k_\mathrm{B} \ln Q = \frac{E}{T} - \frac{A}{T} \tag{2.15}$$

Therefore

$$A(N,V,T) = -k_\mathrm{B}T \ln Q(N,V,T) \tag{2.16}$$

Equation 2.16 allows us to determine entropy, pressure (p), and energy from thermodynamics using

$$dA = -SdT - pdV + \sum_\alpha \mu_\alpha dN_\alpha \tag{2.17}$$

where μ is the chemical potential. Thus,

$$S = -\left(\frac{\partial A}{\partial T} \right)_{V,N} = k_\mathrm{B}T \left(\frac{\partial \ln Q}{\partial T} \right)_{V,N} + k_\mathrm{B} \ln Q \tag{2.18}$$

$$p = -\left(\frac{\partial A}{\partial V} \right)_{T,N} = k_\mathrm{B}T \left(\frac{\partial \ln Q}{\partial V} \right)_{T,N} \tag{2.19}$$

$$E = -T^2 \left(\frac{\partial A/T}{\partial T} \right)_{V,N} = k_\mathrm{B}T^2 \left(\frac{\partial \ln Q}{\partial T} \right)_{V,N} \tag{2.20}$$

2.2 Molecular Simulation Methods

The equations that allow us to compute thermodynamic properties using classical mechanics were given in the previous sections; however, the integrals are frequently impossible to solve due to the complexity of the potential function U and the high dimensionality of the complete set of coordinates and momenta for a molecular system, otherwise known as the "phase space." Fortunately, molecular simulations are a useful tool to bypass direct calculation of the partition function while determining the desired thermodynamic properties. Furthermore, only a small subset of sample configurations, if the simulation samples phase space efficiently, is required for precise calculation of thermodynamic properties.

There are two main techniques for sampling phase space: molecular dynamics (MD) and Monte Carlo (MC). Both techniques have certain advantages and disadvantages when sampling phase space efficiently. In MD, inter- and intra-molecular potentials are used to calculate forces between particles. These forces are then used in Newton's equations of motion to determine how particles move during each timestep, δt. As a result, MD simulations can be used to determine many time-dependent properties such as diffusion rates. To accurately conserve energy and capture high frequency vibrations, δt is typically on the order of a femtosecond or less, which limits the total simulation length to time scales on the order of nanoseconds due to computational cost. Coarse-grained models, which do not contain vibrations with light atoms, permit longer time steps and thus longer simulations at the expense of atomistic detail. Replica-exchange MD is one improvement to help observe phenomena that occur over long time scales such as protein folding [33]. In this method, pairs of replicas from different temperatures are exchanged to move out of local minima on the potential energy surface. Another approach, metadynamics, adds biases to the potential energy surface such that the full energy surface is constant with respect to a set of collective variables [34]. Despite these improvements to MD algorithms, phenomena that occur over long (i.e. millisecond) time spans are still difficult, if not impossible, to observe with current computing technology.

MC simulations instead rely upon probabilities to observe system configurations. The probability to observe a given configuration is proportional to its Boltzmann factor, $e^{-U(\mathbf{q}^N)/k_\mathrm{B}T}$, which results in more frequent sampling of lower energy configurations over higher energy configurations, but lacks time considerations. Thus, MC

is unable to yield precise time-dependent properties; however, unphysical moves are permitted such that high energy barriers can be bypassed and thus rare events are sampled much more efficiently than in MD simulations. In this work, we wish to examine properties which are not time-dependent and unphysical moves can help us sample chain configurations much more efficiently. This technique is explained in greater detail in Section 2.3, and a special scheme for efficient phase space sampling for long chain configurations is explained in 2.5 below.

2.3 Metropolis Monte Carlo

One approach to approximate the integrals in Eqn. 2.11 to calculate our desired thermodynamic properties is known as hit-and-miss integration. Here, N configurations are randomly generated and then the Boltzmann factors for all configurations are summed, and thus the average is computed using the equation:

$$\langle M \rangle \approx \frac{\sum_{j=1}^{J} M(\mathbf{q}_j) e^{-U(\mathbf{q}_j)/k_{\mathrm{B}}T}}{\sum_{j=1}^{J} e^{-U(\mathbf{q}_j)/k_{\mathrm{B}}T}} \tag{2.21}$$

As the $J \to \infty$, Eqn. 2.21 approaches the true ensemble average given in Eqn. 2.11. Since most possible configurations have near-zero Boltzmann factors due to high-energy overlaps between particles, relatively few configurations contribute significantly to the the configuration average and thus contribute to the thermodynamic averages. Given the nature of the hit-and-miss method, a large amount of insignificant configurations is generated, and thus a large amount of computer time is wasted if this technique is used. Fortunately, smarter methods have been developed to increase the likelihood of generating configurations that make a significant contribution to the configuration integral.

The Metropolis Monte Carlo method was used for the first computer simulation in 1953 and remains one of the most popular MC variants to this day [35, 36]. The method also has the moniker "importance" sampling as configurations are chosen according to their Boltzmann weight, but then weighted evenly. As a result, high energy configurations are less likely to be selected, and thus, a smaller total number of configurations can be generated while still obtaining accurate results. This is achieved by starting with a random configuration and undergoing a perturbation upon a single particle (i.e. a translation move) which then puts the system in a new state. This

move is then accepted or rejected according to the Boltzmann weights for the two configurations:

$$P_{\text{acc,old}\rightarrow\text{new}} = \min[1, e^{-\Delta U/k_{\text{B}}T}] \tag{2.22}$$

where ΔU is the change in potential energy between the new and old states. Moves that decrease the potential energy of the system are always accepted. For moves that increase the potential energy, a random number between zero and one is chosen and compared to $e^{-\Delta U/k_{\text{B}}T}$. The move is accepted if the random number is less than $e^{-\Delta U/k_{\text{B}}T}$; otherwise it is rejected and the old configuration is counted again in the averages for the simulation.

Since the original molecular simulations in the 1950's and 1960's, many developments have been made to improve simulation efficiency to allow for sampling of complex chemical systems. These developments include several new algorithms that involve multiple particles in a single move, such as "identity exchange" moves, and algorithms to efficiently sample configurations of long chains. The acceptance rules for these moves must be appropriately modified account for simultaneous changes to multiple particles and the introduction of a bias for improved sampling efficiency.

2.4 The Gibbs Ensemble

The original Metropolis Monte Carlo method can be very useful for determining properties of materials in a single phase; however, many important processes such as separations have multiple phases present that are in thermal, chemical, and mechanical equilibrium with each other. To examine multi-phase systems, the "Gibbs ensemble" was introduced [37, 38, 39]. In the Gibbs ensemble, two or more simulation boxes are utilized, with each box representing a different phase. While there are no explicit interfaces between the boxes, particles and volume (in the NVT ensemble) may be exchanged between the boxes to reach equilibrium. This leads to the NVT-Gibbs ensemble partition function that depends on the number of particles in one of

the boxes, N_1, and the volume of one of the boxes, V_1, shown below:

$$\begin{aligned} Q =& \frac{1}{\Lambda^{3N} N!} \sum_{N_1=0}^{N} \frac{N!}{N!(N-N_1)!} \int_0^V V_1^{N_1} (V - V_1)^{N-N_1} \mathrm{d}V_1 \\ & \times \int \int e^{-U_1(\mathbf{q}^{N_1})/k_\mathrm{B}T} e^{-U_2(\mathbf{q}^{N-N_1})/k_\mathrm{B}T} \mathrm{d}\mathbf{q}^{N_1} \mathrm{d}\mathbf{q}^{N-N_1} \end{aligned} \tag{2.23}$$

The probability density is proportional to the pseudo-Boltzmann weight:

$$\rho \propto \frac{V_1^{N_1} (V - V_1)^{N-N_1}}{N_1!(N-N_1)!} e^{-U_1(\mathbf{q}^{N_1})/k_\mathrm{B}T} e^{-U_2(\mathbf{q}^{N-N_1})/k_\mathrm{B}T} \tag{2.24}$$

This allows us to determine acceptance probabilities as we proceed to sample phase space. First, we will begin with a particle translation in box 1, for which the probability density ratio is given by

$$\frac{\rho_\mathrm{new}}{\rho_\mathrm{old}} = e^{-\Delta U_1(\mathbf{q}^{N_1})/k_\mathrm{B}T} \tag{2.25}$$

where ΔU_1 is the energy difference between the old and new sets of coordinates in box 1. This leads to an acceptance rule analogous to Eqn. 2.22:

$$P_{\mathrm{acc,old}\to\mathrm{new}} = \min[1, e^{-\Delta U(\mathbf{q}^{N_i})/k_\mathrm{B}T}] \tag{2.26}$$

In this work, the systems are designed using an implicit solvent for the polymer chains allowing us to avoid more expensive volume moves. Particle swap moves are used to exchange the chains between the mobile and stationary phases. For the the acceptance rule below, let us consider moving a particle from box 1 into box 2. For the "new" state, the number of particles in box 1 is $N_1 - 1$ and the number of particles in box 2 is $N - N_1 + 1$, so the probability ratio is given by:

$$\begin{aligned} \frac{\rho_\mathrm{new}}{\rho_\mathrm{old}} =& \left(\frac{N_1!(N-N_1)!}{(N_1-1)!(N-N_1+1)!} \right) \left(\frac{V_1^{N_1-1}(V-V_1)^{N-N_1+1}}{V_1^{N_1}(V-V_1)^{N-N_1}} \right) \\ & \times e^{-[\Delta U_1(\mathbf{q}^{N_1}) + \Delta U_2(\mathbf{q}^{N-N_1})]/k_\mathrm{B}T} \\ =& \left(\frac{N_1}{N-N_1+1} \right) \left(\frac{V-V_1}{V_1} \right) e^{-[\Delta U_1(\mathbf{q}^{N}) + \Delta U_2(\mathbf{q}^{N})]/k_\mathrm{B}T} \end{aligned} \tag{2.27}$$

where

$$\Delta U_1(\mathbf{q}^N) = U_1(\mathbf{q}^{N-N_1}) - U_1(\mathbf{q}^{N_1}) \tag{2.28}$$

and

$$\Delta U_2(\mathbf{q}^N) = U_2(\mathbf{q}^{N-N_1+1}) - U_2(\mathbf{q}^{N-N_1}) \tag{2.29}$$

This leads to the acceptance rule

$$P_{\text{acc,old}\to\text{new}} = \min\left[1, \left(\frac{N_1}{N-N_1+1}\right)\left(\frac{V-V_1}{V_1}\right) \times e^{-[\Delta U_1(\mathbf{q}^N)+\Delta U_2(\mathbf{q}^N)]/k_\text{B}T}\right] \tag{2.30}$$

This particular acceptance rule only applies to single bead particle or rigid molecule simple swap moves where only one trial site is used. It is much more efficient to use multiple trial insertion sites, particularly with long, flexible chains such as the polymers studied in this work. The configurational-bias Monte Carlo algorithm allows us to use multiple insertion sites and change the conformation of a chain in combination with a swap move. This algorithm is discussed in more detail in the next section.

2.5 Configurational-bias Monte Carlo

The original simple MC moves such as translation and rotation work fairly well for sampling phase space for a system of rigid or single-bead particles; however, multi-bead chains need additional moves to sample the added degrees of freedom. One approach is to perform atom translations upon individual beads within the chain; however, this often leads to unfavorable bond lengths, bond angles, or torsions within the chain and thus many of these moves are rejected which leads to more costly simulations. To help address this issue, Rosenbluth and Rosenbluth proposed a self-avoiding walk algorithm for growing a polymer chain on a lattice [40]. As computers improved and more simulations were performed in continuous space, configurational-bias Monte Carlo (CBMC) was developed in the 1990's [41, 42, 43, 44, 45]. This algorithm samples chain configurations much more efficiently by generating trial configurations in such a way that the chain avoids itself and other chains in the system, while accounting for intramolecular potentials.

A CBMC move occurs in several steps which include chain selection, new configuration growth, old configuration regrowth, and accepting or rejecting the move. In CBMC, it is more efficient to separate the interactions such that bonded interactions (U^int) are used to generate trial site, and non-bonded interactions (U^ext) are used

to bias the selection of the trial site [46]. A separation of inter- and intra-molecular interactions is required to correctly sample configurations for branched architectures, but considering bonded interactions for trial site generation or for trial site selection is valid.

In the first step of a CBMC move, a chain segment is selected randomly and then all segments between the selected segment and either one of the chain ends are discarded. Then, the discarded segments are regrown sequentially from the chain fragment that was not discarded. The first regrowth step consists of generating *nchoice* trial sites for the first bead where the probability to select a site is influenced by its Rosenbluth weight, $w_1$new, which is given by

$$w_1(\text{new}) = \sum_{j=1}^{nchoice} \exp[-U_{1j}^{\text{ext}}/k_{\text{B}}T] \tag{2.31}$$

which is used to calculate the probability to select a site i with

$$P_{1i} = \frac{\exp[-U_{1i}^{\text{ext}}/k_{\text{B}}T]}{w_1(\text{new})} \tag{2.32}$$

For each sequential segment, l, *nchoice* trial positions are generated and have a Rosenbluth weight given by

$$w_l(\text{new}) = \sum_{j=1}^{nchoice} \exp[-U_{lj}^{\text{ext}}/k_{\text{B}}T] \tag{2.33}$$

with the probability of selecting trial site i determined by

$$P_{l,i} = \frac{\exp[-U_{l,i}/k_{\text{B}}T]}{\sum_{j=1}^{nchoice} \exp[-U_{l,j}/k_{\text{B}}T]} \tag{2.34}$$

The iterative growth process is repeated for all segments that need to be regrown, n_{grow}, which results in a Rosenbluth weight, W, for the regrowth given by:

$$W_{\text{new}} = \prod_{l=1}^{n_{\text{grow}}} \frac{1}{n} \sum_{i=1}^{n} \exp[-U_{l,i}/k_{\text{B}}T] \tag{2.35}$$

This scheme is much more efficient for sampling configurations as chains are preferentially grown in favorable configurations based on their surroundings; however, this bias needs to be removed when determining whether to accept or reject the move. Therefore, we need the Rosenbluth weight for the old configuration, W_{old}.

This is performed with an analogous iterative growth procedure. First, $f-1$ trial sites are randomly generated and the f^{th} site corresponds to the old configuration. The Rosenbluth weight for the first segment of the old configuration is given by

$$w_1(\text{old}) = \sum_{j=1}^{f-1} \exp[-U_{1j}^{\text{ext}}/k_{\text{B}}T] + \exp[-U_{1f}^{\text{ext}}/k_{\text{B}}T] \tag{2.36}$$

where $\exp[-U_{1f}^{\text{ext}}/k_{\text{B}}T]$ is the actual potential energy from nonbonded interactions for the first segment in the old configuration. For each of the remaining segments, an analogous procedure is followed in which $nchoice-1$ trial sites are generated and the Rosenbluth weight of each segment l is given by

$$w_1(\text{old}) = \sum_{j=1}^{k-1} \exp[-U_{lj}^{\text{ext}}/k_{\text{B}}T] + \exp[-U_{lk}^{\text{ext}}/k_{\text{B}}T] \tag{2.37}$$

where $\exp[-U_{lk}^{\text{ext}}/k_{\text{B}}T]$ is the actual potential energy from nonbonded interactions for segment l in the old configuration.

Now that Rosenbluth weights for both configurations have been determined, the move can be accepted according to

$$P_{\text{acc,old}\to\text{new}} = \min\left[1, \frac{W_{\text{new}}}{W_{\text{old}}}\right] \tag{2.38}$$

It has been shown that this acceptance rule properly samples the Boltzmann distribution for linear chains [41, 42, 43, 44, 45].

In addition to sampling chain configurations, this algorithm can be used to improve swap moves for flexible chains between phases as it inserts a molecule bead by bead so that configurations with overlaps are avoided. When applied to a swap move, the CBMC method first finds a location for the first bead of the molecule. This is done by placing the first bead at $nchoi1$ trial sites and selecting one with a probability given by:

$$P_{1,i} = \frac{\exp[-U_i/k_{\text{B}}T]}{\sum_{j=1}^{n} \exp[-U_j/k_{\text{B}}T]} \tag{2.39}$$

where U_j is the potential energy of the first bead, at position j with all other molecules in the new box. After the first bead is inserted, the scheme given in Eqn. 2.34 is followed for the rest of the chain insertion. Like with partial chain regrowth, the Rosenbluth weight of the old configuration is determined by repeating this scheme

to generate the old configuration. The weights for the new configuration, W_{ins}, and the old configuration, W_{old}, are used to calculate the probability to accept the swap move determined by:

$$P_{\text{acc,old}\to\text{new}} = \min\left[1, \frac{N_1}{N_2+1}\frac{V_2}{V_1}\frac{W_{\text{ins}}}{W_{\text{old}}}\right] \tag{2.40}$$

Several years after the CBMC was first published, Vlugt and Smit found that the distribution of angles was not correctly sampled if only the bonded interactions are considered when growing branched chains with CBMC [47]. This can be remedied by including the bond bending, torsional energies, and the interatomic potential energy (i.e. a Lennard-Jones type potential) when growing a molecule. Unfortunately, this method is quite inefficient as it requires a large number of sample positions to obtain suitable bending angles; thus, a significant number of Lennard-Jones energies must be calculated. To address this problem, the coupled-decoupled CBMC algorithm was introduced [46]. In this variant of CBMC, the bond angles are sampled separately from torsion and Lennard-Jones energy sampling, but the Rosenbluth weight from the bond angle selection is propagated through for the final acceptance probability. As a result, a large number of bond angles may be sampled without significantly increasing the cost of the simulation.

Chapter 3

Linear Copolymers in LCCC

3.1 Introduction

As discussed in Chapter 1, many separation techniques are used to characterize polymers, among which size exclusion chromatography (SEC) is the most popular. SEC separates polymers predominately by their molecular size (e.g., hydrodynamic volume, radius of gyration, or mean span dimension) [48, 49], and it is used in the fractionation and characterization of polymers, from homopolymers to complex block copolymers with unique molecular topologies [5]. Previous work in SEC has shown that entropic effects (i.e., confinement reducing the number of conformations accessible to the polymer) are primarily responsible for separation, but enthalpic effects also play a nuanced role [5, 50, 51, 52]. The traditional experimental SEC methodology uses standards or calibration curves to aid in the determination of the molecular weight distribution and works fairly well for homopolymers, but complications arise when copolymers are analyzed as different monomer sequences have different hydrodynamic volumes in the same solvent [4, 6]. Interest in multicomponent polymers has surged with promising applications in drug delivery, microelectronics, and other advanced materials [3]. This interest has led to numerous techniques to synthesize multicomponent and multiblock copolymers, and understanding how to properly characterize these more complex polymers is crucial [3].

Liquid chromatography techniques, such as reversed-phase liquid chromatography, are also used to characterize polymers. The affinity of the polymer to adsorb or

(partially) partition into the bonded phase or for "bonding" to specific strong adsorption sites plays a significant role in determining retention order. LCCC is positioned at the interface of these affinity-based techniques and SEC. LCCC finds tremendous utility in the characterization of the molecular-weight distribution of block copolymers [4, 6]. In LCCC, operating conditions are chosen to have homopolymers co-elute independent of their molecular weight. The critical condition is the combination of unique temperature and solvent composition such that the incremental transfer free energy per segment becomes zero and, therefore makes the differences in molecular weight chromatographically "invisible." When analyzing copolymers, the operating parameters are set to the critical condition of one monomer type and separation is mostly dependent on the molecular weight of the other monomer types. This process can be repeated for the other component(s) to determine the molecular-weight distributions for all components when either mass spectrometry and/or suitable polymer standards are available. However, multi-dimensional chromatographic methods would still be needed to determine how the different weight fractions are coupled to form the copolymers. Another important question concerns the topology of copolymers. Given the rise of multiblock copolymers such as triblocks or tetrablocks [3], it is necessary to confirm whether monomer sequence affects LCCC retention of linear copolymers.

Experimental studies of block copolymers have sometimes yielded conflicting conclusions regarding sequence effects on retention. In an earlier study, Falkenhagen et al. [7, 8] reported co-elution for diblocks of poly(methyl methacrylate) and poly(*tert*-butyl methacrylate) and triblocks with the invisible end blocks and surmised that the amount of visible monomer within a polymer chain determined from LCCC is not strongly influenced by monomer sequence. In contrast, Lee et al. [53] reported that a block does not become completely invisible at the critical condition of the corresponding homopolymer and that polystyrene-*b*-polyisoprene diblocks elute before the homopolymer when both have the same number of visible segments. For polystyrene/polybutadiene block copolymers, Park et al. [9] observed that the triblock sequence with the invisible polybutadiene as the middle block elutes significantly earlier than the triblock sequence with the invisible blocks at the end of the diblock sequence, where the latter two elute together. In a more recent study of polystyrene and poly(2-vinylpyridine) copolymers, Cho et al. [54] found that the triblock sequence with invisible end blocks elutes after a comparable diblock, i.e., that the shorter end

blocks have a slightly more effective interaction with the stationary phase than the longer block of the diblock copolymer.

Several simulation studies have examined the behavior of linear polymer chains partitioning between a bulk solution and a slit pore in the interest of examining the critical condition [23, 24, 25, 26, 28, 55]. These studies examined random and self-avoiding walks on a lattice. The partition constants were determined from the chemical potentials of the chains in each environment, and the critical condition was chosen as the bead-wall interaction strength that minimizes the standard deviation of the logarithm of the partition constant[26, 28]. These studies found that the critical condition depends on the slit width for a self-avoiding walk, but tends to the critical adsorption point as the slit width increases [23, 24, 25, 26, 28]. More complex substrate geometries, such a column substrates with corners and edges, require adjustments in the bead-wall interactions to approach LCCC behavior [55].

Systems of random and block copolymers partitioning into a slit pore have been simulated as well by Wang and co-workers [27, 30, 49]. The critical condition for statistically random copolymers was found to depend on both chemical composition and sequence order; hence, the chromatographic resolution is impaired when the sequence order or composition distribution is broad [49]. For block copolymers with the invisible **B** monomer, it was found that the partition constants for the **AB** diblock and **BAB** triblock copolymers are larger than those of a homopolymer with the same number of **A** monomers, whereas the partition constants for the **ABA** triblock copolymer are smaller than those of the homopolymer [27, 30]. Such sequence effects can lead to incorrect estimation for the molecular weight (distribution) of block copolymers [27].

The current computational work expands upon the work of Wang and co-workers who used lattice models partitioning into planar slit and square channel pores [25, 26, 28, 27, 30, 49, 55]. Here, off-lattice, freely-jointed linear polymers partitioning between a bulk mobile phase and either a spherical pore or a cylindrical pore are investigated, and the partition constants are directly calculated from the average number densities of the polymers in the two environments.

3.2 Computational Details

The Gibbs ensemble Monte Carlo (GEMC) method [37, 38], involves two simulation boxes and allows for the efficient calculation of phase and sorption equilibria [56], and has also been applied for numerous chromatographic systems [57]. Here, the GEMC simulations employ the configurational-bias Monte Carlo algorithm [42, 58, 59] to sample chain conformations and assist with particle transfer moves between the two boxes, one box containing the mobile phase and the other box representing the stationary phase as either a spherical or cylindrical pore. Only one polymer chain is used in each simulation to mimic the infinite-dilution limit, and the solvent is treated implicitly. Thus, there is no need to sample volume fluctuations during the GEMC simulations. Here, equal proportions of configurational-bias Monte Carlo moves are used to sample conformational degrees of freedom within a given phase and for particle transfers between the phases.

Each block copolymer is represented by a chain of freely-jointed beads with a diameter of σ and the total number of beads in a chain is designated by N. All bead-bead interactions are described by a hard sphere potential, and consequently the solvent does not distinguish between the two monomer types. All copolymers consist of equal proportions of **A** and **B** type monomers arranged in five sequences: diblock, two triblock (both **ABA** and **BAB** arrangements), tetrablock, and alternating (see Figure 3.1).

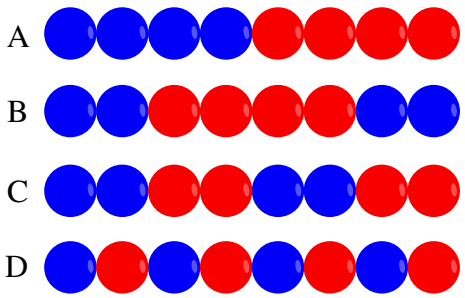

Figure 3.1: Illustrations of **AB** diblock (A), **ABA** triblock (B), **ABAB** tetrablock (C), and alternating (D) sequences for copolymers with $N = 8$.

To decide on a suitable pore diameter, the radius of gyration, R_g, for a chain

length is calculated as follows:

$$R_{\mathrm{g}} = \sqrt{\frac{1}{N}\sum_{k=1}^{N}(\mathbf{r}_k - \mathbf{r}_{\mathrm{COM}})^2} \tag{3.1}$$

where $\mathbf{r}_{\mathrm{k}}$ and $\mathbf{r}_{\mathrm{COM}}$ are the positions of the k-th bead and of the center of mass, respectively. Configurational-bias Monte Carlo simulations yield $R_{\mathrm{g}}/\sigma = 3.609 \pm 0.001$, 5.599 ± 0.001, 8.606 ± 0.003, and 13.14 ± 0.02 for chains of lengths 32, 64, 128, and 256, respectively (with standard error of the mean provided). These R_{g} values can be described well by a scaling law ($R_{\mathrm{g}} \propto N^{\nu}$) and yield a Flory exponent of $\nu = 0.62 \pm 0.004$ that indicates that the freely-jointed bead model represents a polymer in a good solvent [60]. Based on the R_{g} for the longest polymer investigated here ($N = 256$), a pore diameter of 40σ which falls within the typical size exclusion regime, is chosen for both the spherical and cylindrical pores [5]. For the cylindrical pore, the periodic boundary condition is applied along its long axis, with the length set to $L_{\mathrm{cyl}}/\sigma = N + 1$ to allow for the (unlikely) case of a fully extended chain. Similarly, the size of the mobile-phase box is varied with chain length to permit the fully extended chain conformation ($L_{\mathrm{mob}}/\sigma = N + 1$).

Two different interaction potentials are used to describe segment–pore wall interactions. For bead type **A**, a hard-sphere potential is used that prevents segment–wall overlaps, while a square-well potential is used for bead type **B** that also prevents segment–wall overlaps but provides a favorable interaction energy when a bead is located within one bead diameter of the pore wall. The square-well potential is as follows:

$$u_{\mathbf{B}}(r) = \begin{cases} \infty & \text{for} \quad r \geq 20\sigma \\ -\epsilon & \text{for} \quad 19\sigma \leq r < 20\sigma \\ 0 & \text{for} \quad r < 19\sigma \end{cases} \tag{3.2}$$

where r is the radial distance from the center of the pore. The well depth to absolute temperature ratio, $\epsilon/k_{\mathrm{B}}T$, can be adjusted to yield the critical condition.

The determination of the critical condition for **B** homopolymers is carried out in two stages. The first is a broad sweep over a wide range of $\epsilon/k_{\mathrm{B}}T$ values, which uses simulations consisting of 12×10^6 Monte Carlo steps for each condition. Once the approximate critical condition is found, the second stage uses eight independent simulations, each consisting of 18×10^6 Monte Carlo steps for each $\epsilon/k_{\mathrm{B}}T$ value in a narrow range to assess the critical condition with greater precision.

Once the critical condition was determined, the simulations for the block copolymers and both homopolymers consist of 24×10^6 Monte Carlo steps with eight independent simulations performed for $N \leq 128$, while 32 and 72 independent simulations are used for $N = 256$ to account for the lower acceptance rate of particle transfer moves in the cylindrical and spherical pores, respectively. Information from each Monte Carlo step is used to compute the partition constant from the ratio of the number densities in the pore versus the mobile phase. The chain configurations are stored every 200 cycles to allow for the calculation of structural properties. Statistical uncertainties are given as the standard error of the mean, unless noted otherwise, and are calculated using data from independent simulations.

To improve statistics for the computation of the partition constant, a biasing potential is utilized for each simulation so that the copolymer chain spends roughly equal proportions of the simulation trajectory in each phase, but this biasing potential is removed when calculating the partition constant [61].

3.3 Results and Discussion

3.3.1 Determination of the Critical Condition

The critical condition for the spherical pore is estimated by calculating the retention factors, K, for **B** homopolymers of different lengths for a range of segment–wall interaction strengths (or, correspondingly, inverse temperatures). The K values obtained for $\epsilon/k_{\mathrm{B}}T$ ratios from 0.0 to 0.9 (in increments of 0.1) are depicted in Figure 3.2. For $\epsilon/k_{\mathrm{B}}T = 0.0$, the pore is acting in a purely exclusionary mode, and, therefore, longer chain lengths have a lower K due to the increased entropic penalty associated with transferring into the pore. For $\epsilon/k_{\mathrm{B}}T \leq 0.3$, the retention factors greatly decrease with increasing chain length; i.e., the system is in the SEC regime. Near $\epsilon/k_{\mathrm{B}}T \approx 0.4$, steric exclusion and affinity are balanced, leading to co-elution of different length chains. The system enters the liquid adsorption (affinity) chromatography regime at $\epsilon/k_{\mathrm{B}}T \geq 0.5$, with increasing separation as the $\epsilon/k_{\mathrm{B}}T$ ratio increases.

To assess the near-LCCC regime in greater detail, more precise retention factors are determined for $\epsilon/k_{\mathrm{B}}T$ ratios falling into the range from 0.36 to 0.43 for the spherical pore and from 0.35 to 0.42 for the cylindrical pore. Figure 3.3 displays the K values obtained from these simulations. Polynomial fits to the K values for a given N

versus the $\epsilon/k_{\mathrm{B}}T$ ratio indicate that there is no unique intersection point for the six and four chain lengths considered for the spherical and cylindrical pores, respectively. Thus, a strict critical condition does not exist in agreement with previous simulation studies [26, 28, 55]. For each pair of consecutive chain lengths, the intersection point is shifted towards larger $\epsilon/k_{\mathrm{B}}T$ ratios. This occurs because as the chain length increases, the fraction of pore wall surface not occupied by other chain segments decreases so there is a greater entropic penalty for a segment of type **B** belonging to a longer chain to adsorb at the pore wall. This increasing entropic penalty necessitates a larger enthalpic gain to achieve the same retention factor for pairs of longer chains.

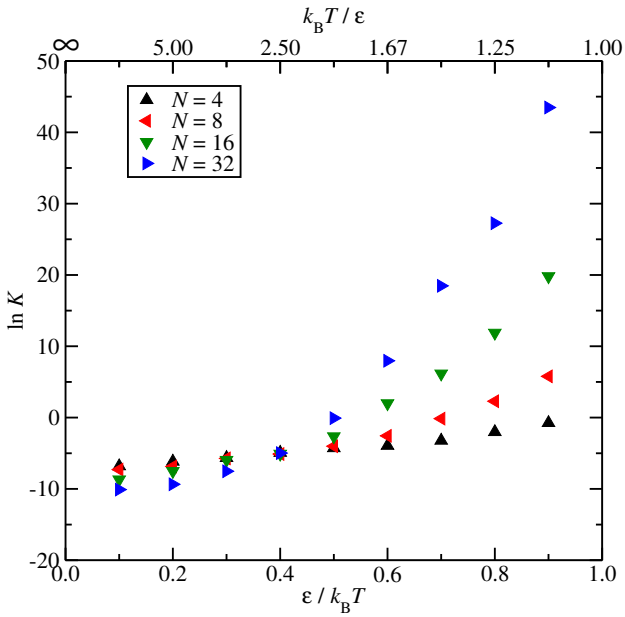

Figure 3.2: Logarithm of the retention factors for **B** homopolymers with $4 \leq N \leq 32$ in the spherical pore versus strength of segment–wall interaction (or inverse temperature).

Comparing the intersection points obtained from polynomial fits for the systems with spherical and cylindrical pores (see Table 3.1), it becomes apparent that the $\epsilon/k_{\mathrm{B}}T$ ratios are systematically shifted to slightly lower values for the cylindrical pore compared to the spherical pore; i.e., the entropic penalty is somewhat smaller for the cylindrical pore as one should expect for chains being confined in only two dimensions instead of three for the spherical pore. Given that real chromatographic systems contain a distribution of pore diameters and shapes, a common segment–wall

strength of $\epsilon/k_{\mathrm{B}}T = 0.40$ is chosen here for bead type **B** as a close approximation to the critical condition.

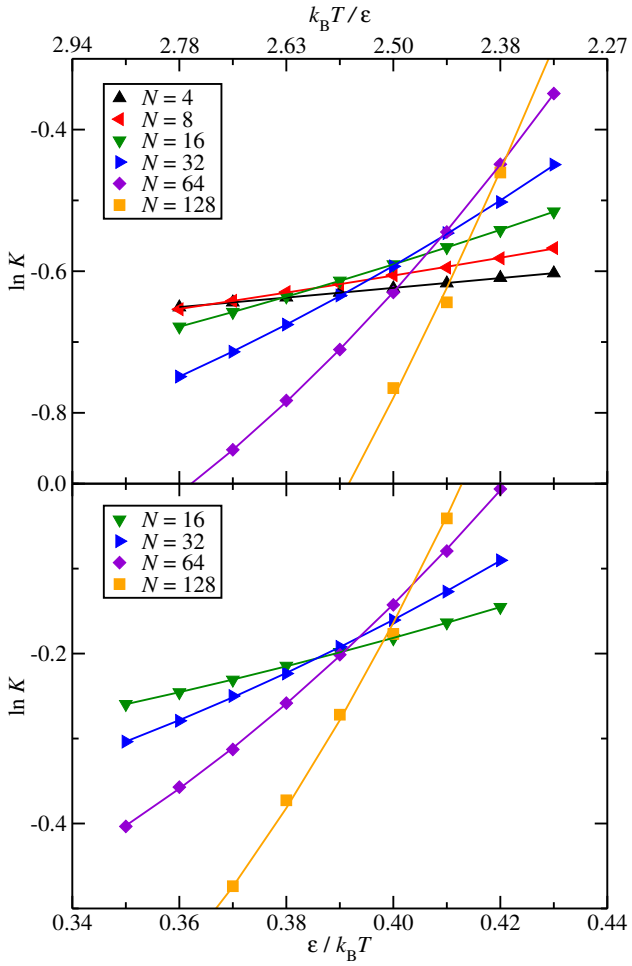

Figure 3.3: Near-LCCC region showing the logarithm of the retention factors for **B** homopolymers with $4 \leq N \leq 128$ in the spherical (top) and cylindrical (bottom) pores versus strength of segment–wall interaction (or inverse temperature). Lines represent second-order polynomial fits.

Table 3.1: Intersection $\epsilon/k_{\mathrm{B}}T$ ratios for each pair of consecutive chain lengths. "SPH" and "CYL" indicate partitioning into a spherical or cylindrical pore, respectively.

N_1	N_2	SPH	CYL
4	8	0.366	–
8	16	0.386	–
16	32	0.403	0.386
32	64	0.408	0.394
64	128	0.421	0.404

3.3.2 Retention Behavior of Copolymers

The retention factors of the five different types of copolymers partitioning into the spherical and cylindrical pores are calculated for chain lengths ranging from 32 to 256 total segments and are displayed in Figure 3.4. Also shown are the retention factors for **A** and **B** type homopolymers. In LCCC, it is usually assumed that the invisible segments do not contribute to retention and, hence, the K value of a copolymer should be equal to that of a homopolymer with the same number of **A** segments. Specifically, for a copolymer with equal proportions of **A** and **B** segments, the retention factor would be as follows [5]:

$$\ln K_{\mathrm{AB},\,N} = \ln K_{\mathbf{A},\,N/2} \tag{3.3}$$

where the labels AB and **A** denote AB copolymer (irrespective of sequence) and **A** hompolymer, respectively, and N is the total number of segments for these polymers.

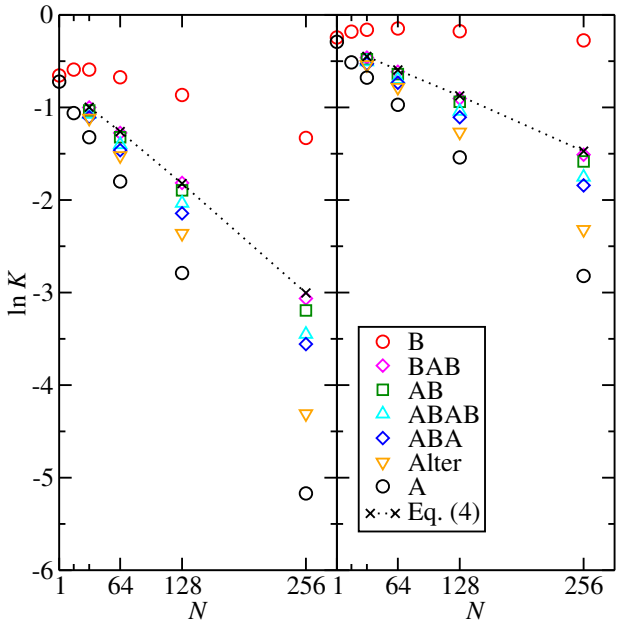

Figure 3.4: Logarithm of the retention factors for polymers in the spherical (left) and cylindrical (right) pores as function of chain length. Error bars are smaller than the symbol size. The dashed line shows the predicted values calculated from Equation 3.4.

However, as discussed above, a strict critical condition does not exist and the K values for the **B** homopolymer are found to be a non-monotonic function of N. For short chains, the K value of the **B** homopolymers increases with N because the entropic cost for interacting with the pore wall is smaller when only a small fraction of the pore surface is occupied by polymer segments. The maximum in K is found for a different N value in the spherical and cylindrical pore systems because the increase in entropic penalty for segment–wall interactions is larger in the more confining spherical pore. This effect also leads to a steeper negative slope in the $\ln K$ values for **B** homopolymers upon further increase in N for the spherical pore. Such a non-linear variation of K with chain length has also been observed for self-avoiding random walks near the critical adsorption condition [62].

Although the $\ln K$ values of the **A** homopolymer can be described well by a linear fit for $N \leq 128$, the $\ln K$ value for $N = 256$ falls significantly below this fit because the entropic size exclusion penalty rapidly increases as R_g becomes greater than 40% of the pore diameter. Taking the non-monotonic behavior for the **B** homopolymer

and the non-linear behavior for the **A** homopolymer into account, the retention factor of a copolymer with equal numbers of **A** and **B** segments and total length N can be estimated as follows:

$$\ln K_{\mathrm{AB},\,N} = \ln K_{\mathbf{A},\,N/2} + \ln K_{\mathbf{B},\,N/2+1} - \ln K_{\mathbf{B},\,1} \tag{3.4}$$

The contribution from type **B** segments is split into two parts to avoid double-counting the translational entropy penalty for placing a particle in the pore that is already included in $\ln K_{\mathbf{A},\,N/2}$. It should be noted that Equations 3.3 and 3.4 predict copolymer retention factors that are independent of sequence. For the specific data points shown for Equation 3.4 in Figure 3.4, the $\ln K_{\mathbf{A},\,N/2}$ and $\ln K_{\mathbf{B},\,1}$ values are taken directly from the simulations, while the $\ln K_{\mathbf{B},\,N/2+1}$ values are determined from a local fit to the two nearest $\ln K_{\mathbf{B}}$ values. In general, these local fits are also used when reversing Equation 3.4 to determine $N_{\mathbf{A}}$ from a "measured" $\ln K_{\mathrm{AB}}$ value of a copolymer.

For all N values investigated here, the retention factors exhibit a significant sequence dependence; this is neither accounted for by Equations 3.3 nor 3.4. The spherical and cylindrical pores yield the same retention order (from least to most retained): alternating, **ABA** triblock, tetrablock, diblock, and **BAB** triblock. The spread in the K values for copolymers differing only in sequence is larger for the spherical than the cylindrical pore, as one may expect from the stronger confinement in a spherical pore of the same diameter.

The K values for the alternating sequence are significantly smaller than those of the block sequences. At first, this may be surprising as this sequence could be viewed as a chain of (AB) beads where the (AB) bead should have properties intermediate to those of **A** and **B** beads. Excluding the triblocks, the K values are found to decrease with increasing number of **AB** connections (from diblock over tetrablock to alternating); i.e., each connection adds an entropic penalty for neighboring **B** segments to interact with the pore wall. Considering the much larger number of **AB** connections in an alternating copolymer, it is now obvious why a larger decrease in K is found.

The observation that the **BAB** triblock copolymer is slightly stronger retained than the diblock copolymer indicates that the proximity of **B** segments to the chain termini plays a role. In contrast, placing the **B** block in the center, as for the **ABA** triblock, significantly decreases retention. The microscopic origins for the sequence dependence will be discussed in detail in Section 3.3.4. The trends in retention order

for the diblock and triblock sequences matches experimental results by Park et al. [9] and Cho et al. [54] Lattice Monte Carlo calculations by Jiang et al. [27] for copolymers with equal proportions of **A** and **B** monomers near LCCC yielded an artificially high **A** length for the **ABA** triblock while the **BAB** triblock had an artificially low **A** length, also indicating that **ABA** copolymers are retained less than **BAB** copolymers [27].

3.3.3 Internal Energy and Entropic Contributions

To determine the thermodynamic factors that govern retention, additional simulations were carried out over a narrow temperature interval spanning $0.95\,T_{\mathrm{LCCC}} \leq T \leq 1.05\,T_{\mathrm{LCCC}}$ where $T_{\mathrm{LCCC}} = 0.4\epsilon/k_{\mathrm{B}}$ is the temperature corresponding to the critical condition. The internal energy, $\Delta U_{\mathrm{trans}}$, and entropy, $\Delta S_{\mathrm{trans}}$, of transfer from the solution phase to the pore were determined from the van't Hoff equation:

$$\ln K = -\frac{\Delta U_{\mathrm{transfer}}}{k_{\mathrm{B}}T} + \frac{\Delta S_{\mathrm{transfer}}}{k_{\mathrm{B}}} \tag{3.5}$$

where a weighted linear regression fit to $\ln K$ plotted as a function of $\epsilon/k_{\mathrm{B}}T$ yields both $\Delta U_{\mathrm{trans}}$ and $\Delta S_{\mathrm{trans}}$ from the slope and intercept, respectively. (Note that $\Delta U_{\mathrm{trans}} = \Delta H_{\mathrm{trans}}$ when the partial molar volume of the polymer is the same in the solution phase and in the pore.)

The van't Hoff plots (see Figure 3.5) again illustrate that both spherical and cylindrical pores yield the same retention order over this entire temperature range. However, the slopes indicate that $\Delta H_{\mathrm{trans}}$ is larger for the spherical than for the cylindrical pore despite that the same bead-wall interactions are used for both pores. The values of the intercepts show that, as expected, $\Delta S_{\mathrm{trans}}$ is significantly larger in magnitude for the spherical than the cylindrical pore due to greater confinement. The data for the diblock, the two triblocks, and the tetrablock copolymers are clustered together, whereas those for the alternating (only for $N = 256$) and the two homopolymers are well separated.

The internal energy and Helmholtz energy of transfer determined for each temperature may be used to determine the entropy of transfer with the equation [63]:

$$T\Delta S_{\mathrm{trans}} = \Delta U_{\mathrm{trans}} - \Delta A_{\mathrm{trans}} \tag{3.6}$$

The internal energy of transfer, Helmholtz energy of transfer, and entropy of transfer obtained from Equations 3.5 and 3.6 are given in Tables 3.2, 3.3, 3.4, 3.5 for polymers partitioning into the spherical for $N = 32$, 64, 128, and 256, respectively. These properties of transfer for polymers partitioning into the cylindrical pore are given in Tables 3.6, 3.7, 3.8, 3.9 for $N = 32$, 64, 128, and 256, respectively. These data for partitioning into the spherical or cylindrical pores are plotted in Figures 3.6 and 3.7, respectively.

A significant temperature dependence is seen for all three properties calculated from Eq. 3.6. Furthermore, different values are seen for each polymer sequence. The two homopolymers, and the alternating copolymer are each significantly different from the cluster containing the other block copolymers.

Neither the internal energy term nor the temperature–entropy term completely dominates the variation in the the Helmholtz energy of transfer. Instead, a compensation between the two terms occurs such that the Helmholtz energy of tranfer appears to be linear with respect to temperature. Entropy is assumed to be constant in Eq. 3.5 and, thus, yields incorrect values for internal energy and entropy of transfer for each of the sequences even though it would appear applicable based solely on the partition constants seen in Fig. 3.5.

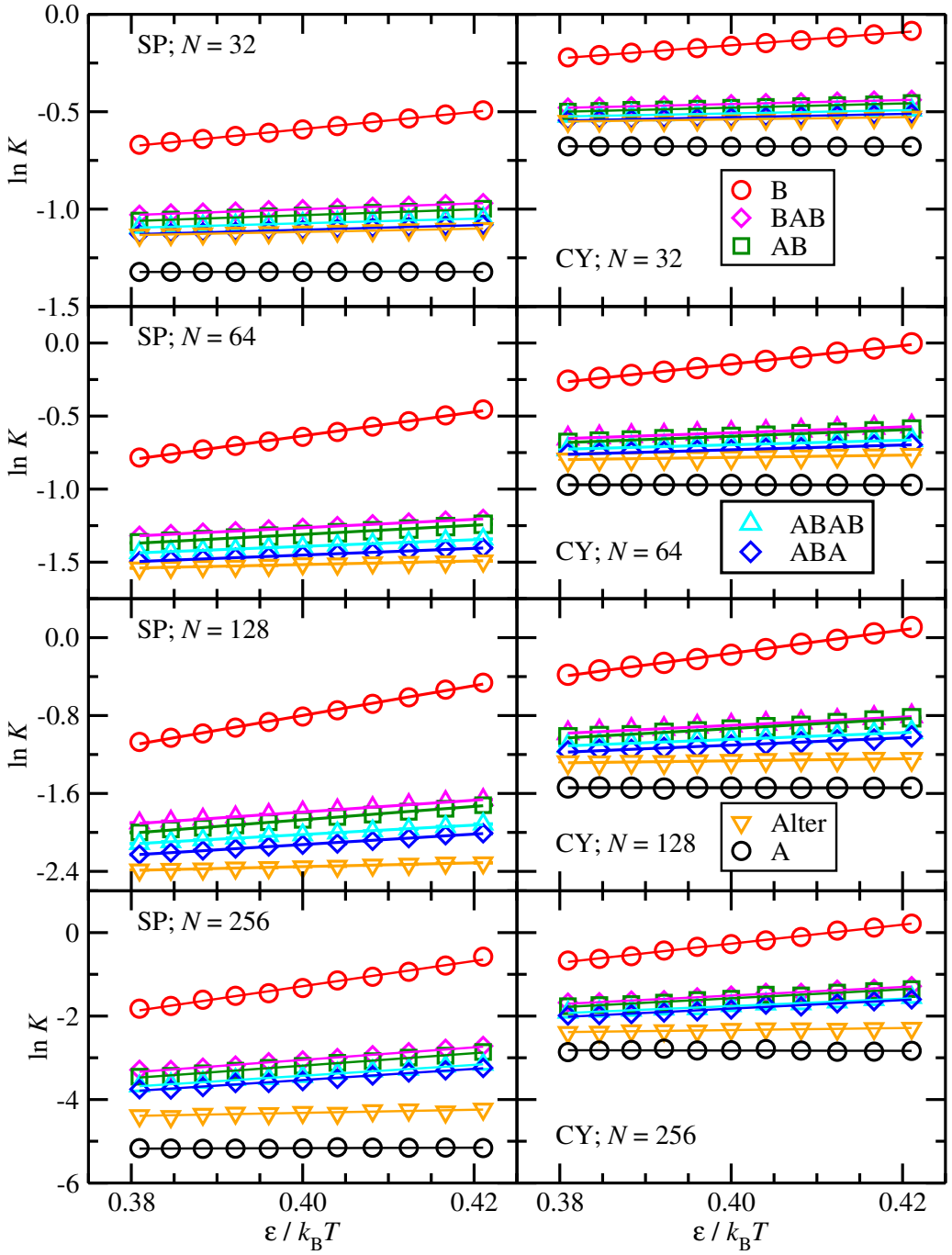

Figure 3.5: Van't Hoff plots for the logarithm of the retention factor as function of inverse temperature for polymers with $N = 32$ (top), $N = 64$ (second from top), $N = 128$ (second from bottom) and 256 (bottom) in the spherical (left) and cylindrical (right) pores. Error bars are smaller than the symbol size. The solid lines show weighted linear fits.

Table 3.2: Internal energies, entropies, and Helmholtz energies of transfer for polymers from the solution phase to spherical pores for $N = 32$. Errors designate standard errors of the mean.

r	Property	**A**	**B**	**AB**	**ABA**	**BAB**	**ABAB**	Alter
0.95	$\Delta U_{\mathrm{trans}}/(\epsilon/k_{\mathrm{B}})$	0	-2.3361_{15}	-0.7975_{7}	-0.4700_{5}	-0.7252_{8}	-0.4784_{7}	-0.3655_{4}
	$\Delta S_{\mathrm{trans}}/(\epsilon/k_{\mathrm{B}})$	-3.3065_{17}	-3.6918_{18}	-3.335_{2}	-3.1972_{15}	-3.1872_{12}	-3.1214_{17}	-3.1353_{12}
	$\Delta A_{\mathrm{trans}}/(\epsilon/k_{\mathrm{B}})$	3.1412_{16}	1.1711_{9}	2.3707_{18}	2.5674_{13}	2.3026_{8}	2.4869_{14}	2.6131_{10}
0.96	$\Delta U_{\mathrm{trans}}/(\epsilon/k_{\mathrm{B}})$	0	-2.2588_{19}	-0.7767_{6}	-0.4684_{7}	-0.7090_{7}	-0.4684_{5}	-0.3596_{3}
	$\Delta S_{\mathrm{trans}}/(\epsilon/k_{\mathrm{B}})$	-3.3021_{13}	-3.638_{2}	-3.322_{2}	-3.1224_{18}	-3.1750_{17}	-3.122_{2}	-3.1332_{13}
	$\Delta A_{\mathrm{trans}}/(\epsilon/k_{\mathrm{B}})$	3.1700_{12}	1.2335_{13}	2.4127_{18}	2.5291_{16}	2.3390_{15}	2.5291_{19}	2.6483_{13}
0.97	$\Delta U_{\mathrm{trans}}/(\epsilon/k_{\mathrm{B}})$	0	-2.182_{2}	-0.7560_{11}	-0.4599_{4}	-0.6947_{5}	-0.4599_{6}	-0.3541_{2}
	$\Delta S_{\mathrm{trans}}/(\epsilon/k_{\mathrm{B}})$	-3.3056_{9}	-3.586_{2}	-3.3122_{19}	-3.119_{2}	-3.1740_{14}	-3.1186_{15}	-3.1308_{9}
	$\Delta A_{\mathrm{trans}}/(\epsilon/k_{\mathrm{B}})$	3.2064_{9}	1.2965_{12}	2.4569_{15}	2.565_{2}	2.3841_{13}	2.5651_{13}	2.6828_{8}
0.98	$\Delta U_{\mathrm{trans}}/(\epsilon/k_{\mathrm{B}})$	0	-2.115_{2}	-0.7370_{8}	-0.4507_{10}	-0.6806_{6}	-0.4507_{4}	-0.3489_{3}
	$\Delta S_{\mathrm{trans}}/(\epsilon/k_{\mathrm{B}})$	-3.3064_{19}	-3.544_{2}	-3.299_{2}	-3.118_{2}	-3.1656_{10}	-3.1179_{19}	-3.1328_{14}
	$\Delta A_{\mathrm{trans}}/(\epsilon/k_{\mathrm{B}})$	3.2403_{19}	1.3585_{10}	2.4958_{18}	2.6048_{18}	2.4217_{8}	2.6048_{19}	2.7212_{13}
0.99	$\Delta U_{\mathrm{trans}}/(\epsilon/k_{\mathrm{B}})$	0	-2.0477_{14}	-0.7201_{10}	-0.4413_{5}	-0.6678_{9}	-0.4413_{5}	-0.3433_{5}
	$\Delta S_{\mathrm{trans}}/(\epsilon/k_{\mathrm{B}})$	-3.3046_{16}	-3.5017_{17}	-3.291_{2}	-3.1156_{18}	-3.1635_{19}	-3.116_{2}	-3.1300_{17}
	$\Delta A_{\mathrm{trans}}/(\epsilon/k_{\mathrm{B}})$	3.2716_{15}	1.4189_{8}	2.5377_{17}	2.6432_{17}	2.4640_{17}	2.643_{2}	2.7554_{16}
1.00	$\Delta U_{\mathrm{trans}}/(\epsilon/k_{\mathrm{B}})$	0	-1.9857_{18}	-0.7021_{10}	-0.4336_{7}	-0.6548_{6}	-0.4336_{3}	-0.3386_{4}
	$\Delta S_{\mathrm{trans}}/(\epsilon/k_{\mathrm{B}})$	-3.305_{2}	-3.463_{2}	-3.2840_{17}	-3.117_{3}	-3.1557_{15}	-3.117_{3}	-3.1317_{14}
	$\Delta A_{\mathrm{trans}}/(\epsilon/k_{\mathrm{B}})$	3.305_{2}	1.477_{2}	2.5820_{15}	2.683_{3}	2.5009_{14}	2.683_{3}	2.7931_{14}
1.01	$\Delta U_{\mathrm{trans}}/(\epsilon/k_{\mathrm{B}})$	0	-1.9269_{18}	-0.6858_{8}	-0.4256_{5}	-0.6427_{4}	-0.4256_{6}	-0.3338_{7}
	$\Delta S_{\mathrm{trans}}/(\epsilon/k_{\mathrm{B}})$	-3.3053_{17}	-3.428_{2}	-3.2715_{16}	-3.1152_{17}	-3.1508_{19}	-3.1152_{10}	-3.1317_{17}
	$\Delta A_{\mathrm{trans}}/(\epsilon/k_{\mathrm{B}})$	3.3384_{17}	1.5357_{8}	2.6185_{14}	2.7207_{17}	2.5396_{19}	2.7207_{8}	2.8293_{16}
1.02	$\Delta U_{\mathrm{trans}}/(\epsilon/k_{\mathrm{B}})$	0	-1.870_{3}	-0.6697_{9}	-0.4182_{5}	-0.6312_{3}	-0.4182_{6}	-0.3288_{3}
	$\Delta S_{\mathrm{trans}}/(\epsilon/k_{\mathrm{B}})$	-3.3065_{18}	-3.395_{3}	-3.2653_{19}	-3.1157_{11}	-3.152_{3}	-3.1157_{14}	-3.1322_{11}
	$\Delta A_{\mathrm{trans}}/(\epsilon/k_{\mathrm{B}})$	3.3726_{18}	1.5930_{11}	2.6609_{17}	2.7598_{10}	2.584_{3}	2.7598_{13}	2.8661_{11}
1.03	$\Delta U_{\mathrm{trans}}/(\epsilon/k_{\mathrm{B}})$	0	-1.8153_{15}	-0.6561_{9}	-0.4113_{7}	-0.6197_{4}	-0.4113_{5}	-0.3246_{3}
	$\Delta S_{\mathrm{trans}}/(\epsilon/k_{\mathrm{B}})$	-3.3074_{13}	-3.363_{2}	-3.2617_{19}	-3.1169_{19}	-3.147_{3}	-3.1169_{9}	-3.1314_{11}
	$\Delta A_{\mathrm{trans}}/(\epsilon/k_{\mathrm{B}})$	3.4066_{13}	1.6485_{15}	2.7034_{17}	2.7991_{18}	2.621_{3}	2.7991_{8}	2.9007_{11}
1.04	$\Delta U_{\mathrm{trans}}/(\epsilon/k_{\mathrm{B}})$	0	-1.7651_{10}	-0.6408_{7}	-0.4040_{6}	-0.6104_{6}	-0.4040_{4}	-0.3206_{3}
	$\Delta S_{\mathrm{trans}}/(\epsilon/k_{\mathrm{B}})$	-3.3035_{18}	-3.3362_{16}	-3.2491_{15}	-3.1140_{18}	-3.1430_{11}	-3.1140_{18}	-3.1336_{13}
	$\Delta A_{\mathrm{trans}}/(\epsilon/k_{\mathrm{B}})$	3.4356_{18}	1.7045_{13}	2.7383_{15}	2.8345_{18}	2.6584_{9}	2.8345_{18}	2.9384_{13}
1.05	$\Delta U_{\mathrm{trans}}/(\epsilon/k_{\mathrm{B}})$	0	-1.7169_{8}	-0.6284_{9}	-0.3976_{5}	-0.5978_{5}	-0.3976_{3}	-0.3162_{2}
	$\Delta S_{\mathrm{trans}}/(\epsilon/k_{\mathrm{B}})$	-3.3064_{18}	-3.3093_{12}	-3.2449_{19}	-3.1130_{17}	-3.1417_{19}	-3.1130_{11}	-3.1338_{10}
	$\Delta A_{\mathrm{trans}}/(\epsilon/k_{\mathrm{B}})$	3.472_{3}	1.7578_{10}	2.7788_{17}	2.8711_{17}	2.701_{3}	2.8711_{11}	2.9743_{11}
Eq. 5	$\Delta U_{\mathrm{trans}}/(\epsilon/k_{\mathrm{B}})$	-0.010_{17}	-4.41_{2}	-1.510_{17}	-1.150_{17}	-1.482_{15}	-1.168_{16}	-0.828_{12}
	$\Delta S_{\mathrm{trans}}/(\epsilon/k_{\mathrm{B}})$	-1.326_{7}	-2.352_{8}	-1.635_{7}	-1.566_{7}	-1.593_{6}	-1.540_{7}	-1.448_{5}

Table 3.3: Internal energies, entropies, and Helmholtz energies of transfer for polymers from the solution phase to spherical pores for $N = 64$. Errors designate standard errors of the mean.

T	Property	**A**	**B**	**AB**	**ABA**	**BAB**	**ABAB**	Alter
	$\Delta U_{\text{trans}}/(\epsilon/k_{\text{B}})$	0	-4.896_{7}	-1.795_{3}	-1.319_{4}	-1.566_{3}	-1.2738_{10}	-0.5761_{12}
0.95	$\Delta S_{\text{trans}}/(\epsilon/k_{\text{B}})$	4.498_{4}	6.291_{10}	4.991_{4}	4.896_{5}	4.659_{5}	4.696_{3}	4.336_{6}
	$\Delta A_{\text{trans}}/(\epsilon/k_{\text{B}})$	4.273_{3}	1.081_{62}	2.946_{3}	3.331_{3}	2.860_{4}	3.188_{3}	3.543_{5}
	$\Delta U_{\text{trans}}/(\epsilon/k_{\text{B}})$	0	-4.635_{3}	-1.708_{4}	-1.218_{4}	-1.5078_{14}	-1.218_{2}	-0.5597_{10}
0.96	$\Delta S_{\text{trans}}/(\epsilon/k_{\text{B}})$	4.492_{4}	6.066_{5}	4.922_{5}	4.649_{5}	4.610_{3}	4.649_{5}	4.329_{4}
	$\Delta A_{\text{trans}}/(\epsilon/k_{\text{B}})$	4.312_{3}	1.188_{3}	3.017_{3}	3.245_{4}	2.918_{3}	3.245_{4}	3.596_{4}
	$\Delta U_{\text{trans}}/(\epsilon/k_{\text{B}})$	0	-4.374_{5}	-1.630_{2}	-1.167_{3}	-1.4422_{12}	-1.1674_{10}	-0.5417_{5}
0.97	$\Delta S_{\text{trans}}/(\epsilon/k_{\text{B}})$	4.496_{2}	5.848_{8}	4.865_{5}	4.614_{4}	4.558_{3}	4.614_{2}	4.312_{2}
	$\Delta A_{\text{trans}}/(\epsilon/k_{\text{B}})$	4.3614_{19}	1.299_{6}	3.089_{5}	3.308_{3}	2.979_{2}	3.3084_{19}	3.641_{2}
	$\Delta U_{\text{trans}}/(\epsilon/k_{\text{B}})$	0	-4.123_{7}	-1.553_{2}	-1.124_{2}	-1.3832_{12}	-1.124_{2}	-0.5252_{10}
0.98	$\Delta S_{\text{trans}}/(\epsilon/k_{\text{B}})$	4.502_{5}	5.638_{9}	4.799_{5}	4.584_{5}	4.513_{4}	4.584_{3}	4.296_{2}
	$\Delta A_{\text{trans}}/(\epsilon/k_{\text{B}})$	4.412_{5}	1.402_{5}	3.150_{4}	3.368_{4}	3.039_{4}	3.3679_{18}	3.6848_{18}
	$\Delta U_{\text{trans}}/(\epsilon/k_{\text{B}})$	0	-3.909_{3}	-1.4807_{17}	-1.080_{2}	-1.334_{3}	-1.080_{3}	-0.5095_{5}
0.99	$\Delta S_{\text{trans}}/(\epsilon/k_{\text{B}})$	4.500_{3}	5.470_{7}	4.742_{5}	4.551_{4}	4.481_{6}	4.551_{4}	4.296_{3}
	$\Delta A_{\text{trans}}/(\epsilon/k_{\text{B}})$	4.455_{3}	1.506_{6}	3.213_{5}	3.425_{3}	3.102_{5}	3.425_{3}	3.744_{3}
	$\Delta U_{\text{trans}}/(\epsilon/k_{\text{B}})$	0	-3.705_{7}	-1.420_{3}	-1.033_{2}	-1.279_{2}	-1.0329_{19}	-0.4938_{9}
1.00	$\Delta S_{\text{trans}}/(\epsilon/k_{\text{B}})$	4.494_{3}	5.310_{8}	4.696_{4}	4.519_{4}	4.444_{4}	4.519_{5}	4.272_{3}
	$\Delta A_{\text{trans}}/(\epsilon/k_{\text{B}})$	4.494_{3}	1.605_{4}	3.276_{3}	3.486_{3}	3.164_{4}	3.486_{4}	3.778_{2}
	$\Delta U_{\text{trans}}/(\epsilon/k_{\text{B}})$	0	-3.519_{6}	-1.355_{3}	-0.9945_{16}	-1.2295_{17}	-0.9945_{12}	-0.4794_{9}
1.01	$\Delta S_{\text{trans}}/(\epsilon/k_{\text{B}})$	4.500_{4}	5.169_{8}	4.645_{5}	4.487_{4}	4.407_{3}	4.487_{4}	4.279_{5}
	$\Delta A_{\text{trans}}/(\epsilon/k_{\text{B}})$	4.545_{4}	1.702_{6}	3.337_{4}	3.537_{4}	3.221_{2}	3.537_{4}	3.843_{5}
	$\Delta U_{\text{trans}}/(\epsilon/k_{\text{B}})$	0	-3.332_{6}	-1.2963_{18}	-0.956_{3}	-1.1861_{16}	-0.9561_{13}	-0.4656_{8}
1.02	$\Delta S_{\text{trans}}/(\epsilon/k_{\text{B}})$	4.494_{6}	5.026_{8}	4.609_{3}	4.470_{5}	4.385_{5}	4.470_{4}	4.276_{3}
	$\Delta A_{\text{trans}}/(\epsilon/k_{\text{B}})$	4.584_{6}	1.794_{5}	3.404_{3}	3.603_{3}	3.287_{5}	3.603_{4}	3.896_{3}
	$\Delta U_{\text{trans}}/(\epsilon/k_{\text{B}})$	0	-3.167_{6}	-1.243_{3}	-0.9150_{18}	-1.1419_{14}	-0.915_{2}	-0.4531_{8}
1.03	$\Delta S_{\text{trans}}/(\epsilon/k_{\text{B}})$	4.499_{2}	4.895_{8}	4.572_{5}	4.436_{5}	4.354_{4}	4.436_{3}	4.265_{2}
	$\Delta A_{\text{trans}}/(\epsilon/k_{\text{B}})$	4.634_{2}	1.875_{6}	3.466_{5}	3.654_{4}	3.343_{3}	3.654_{3}	3.939_{2}
	$\Delta U_{\text{trans}}/(\epsilon/k_{\text{B}})$	0	-3.004_{5}	-1.192_{3}	-0.8850_{19}	-1.099_{2}	-0.8850_{18}	-0.4409_{5}
1.04	$\Delta S_{\text{trans}}/(\epsilon/k_{\text{B}})$	4.498_{3}	4.776_{6}	4.538_{4}	4.415_{4}	4.326_{4}	4.415_{5}	4.263_{4}
	$\Delta A_{\text{trans}}/(\epsilon/k_{\text{B}})$	4.678_{3}	1.963_{3}	3.528_{3}	3.707_{4}	3.400_{4}	3.707_{5}	3.993_{4}
	$\Delta U_{\text{trans}}/(\epsilon/k_{\text{B}})$	0	-2.852_{2}	-1.144_{3}	-0.8526_{19}	-1.0582_{18}	-0.8526_{18}	-0.4275_{5}
1.05	$\Delta S_{\text{trans}}/(\epsilon/k_{\text{B}})$	4.494_{3}	4.675_{4}	4.509_{4}	4.398_{3}	4.306_{4}	4.398_{5}	4.258_{5}
	$\Delta A_{\text{trans}}/(\epsilon/k_{\text{B}})$	4.719_{5}	2.058_{3}	3.591_{3}	3.765_{3}	3.463_{4}	3.765_{5}	4.044_{6}
Eq. 5	$\Delta U_{\text{trans}}/(\epsilon/k_{\text{B}})$	0.00_{3}	-8.16_{7}	-3.13_{4}	-2.28_{3}	-2.89_{3}	-2.30_{3}	-1.21_{4}
	$\Delta S_{\text{trans}}/(\epsilon/k_{\text{B}})$	-1.797_{14}	-3.90_{3}	-2.560_{14}	-2.366_{13}	-2.420_{14}	-2.313_{14}	-2.000_{15}

Table 3.4: Internal energies, entropies, and Helmholtz energies of transfer for polymers from the solution phase to spherical pores for $N = 128$. Errors designate standard errors of the mean.

T	Property	**A**	**B**	**AB**	**ABA**	**BAB**	**ABAB**	Alter
	$\Delta U_{\text{trans}}/(\epsilon/k_{\text{B}})$	0	-10.29_4	-4.396_{13}	-3.453_{15}	-3.899_5	-3.126_9	-1.002_3
0.95	$\Delta S_{\text{trans}}/(\epsilon/k_{\text{B}})$	6.973_7	11.99_4	8.929_{17}	8.658_{18}	8.262_9	8.076_{13}	6.835_9
	$\Delta A_{\text{trans}}/(\epsilon/k_{\text{B}})$	6.625_7	1.10_8	4.087_{10}	4.772_8	3.950_6	4.546_8	5.492_8
	$\Delta U_{\text{trans}}/(\epsilon/k_{\text{B}})$	0	-9.62_3	-4.095_{14}	-2.939_{13}	-3.650_{18}	-2.939_{15}	-0.955_3
0.96	$\Delta S_{\text{trans}}/(\epsilon/k_{\text{B}})$	6.980_8	11.35_3	8.659_{16}	7.912_{15}	8.01_2	7.912_{19}	6.781_7
	$\Delta A_{\text{trans}}/(\epsilon/k_{\text{B}})$	6.701_8	1.282_{11}	4.218_7	4.657_5	4.042_6	4.657_9	5.555_5
	$\Delta U_{\text{trans}}/(\epsilon/k_{\text{B}})$	0	-8.78_3	-3.850_{16}	-2.753_8	-3.463_9	-2.753_{15}	-0.916_3
0.97	$\Delta S_{\text{trans}}/(\epsilon/k_{\text{B}})$	6.990_5	10.59_3	8.439_{18}	7.753_{12}	7.857_{12}	7.753_{17}	6.762_9
	$\Delta A_{\text{trans}}/(\epsilon/k_{\text{B}})$	6.780_5	1.487_{11}	4.336_7	4.767_8	4.158_8	4.767_8	5.643_8
	$\Delta U_{\text{trans}}/(\epsilon/k_{\text{B}})$	0	-8.14_2	-3.571_{11}	-2.590_{17}	-3.230_8	-2.590_9	-0.8750_{18}
0.98	$\Delta S_{\text{trans}}/(\epsilon/k_{\text{B}})$	6.976_7	10.01_2	8.187_{13}	7.607_{19}	7.661_{11}	7.607_{13}	6.732_9
	$\Delta A_{\text{trans}}/(\epsilon/k_{\text{B}})$	6.836_7	1.665_7	4.452_7	4.865_8	4.278_8	4.865_9	5.722_9
	$\Delta U_{\text{trans}}/(\epsilon/k_{\text{B}})$	0	-7.50_3	-3.33_2	-2.40_3	-3.027_8	-2.403_{14}	-0.832_5
0.99	$\Delta S_{\text{trans}}/(\epsilon/k_{\text{B}})$	6.964_8	9.44_3	7.97_3	7.44_3	7.480_{12}	7.444_{15}	6.708_{11}
	$\Delta A_{\text{trans}}/(\epsilon/k_{\text{B}})$	6.895_7	1.846_{11}	4.557_8	4.967_8	4.378_9	4.967_6	5.809_9
	$\Delta U_{\text{trans}}/(\epsilon/k_{\text{B}})$	0	-6.93_4	-3.10_2	-2.255_{14}	-2.837_6	-2.255_9	-0.793_3
1.00	$\Delta S_{\text{trans}}/(\epsilon/k_{\text{B}})$	6.969_9	8.95_4	7.78_2	7.320_{17}	7.313_9	7.320_{11}	6.678_8
	$\Delta A_{\text{trans}}/(\epsilon/k_{\text{B}})$	6.969_9	2.025_9	4.678_9	5.065_{10}	4.476_6	5.065_6	5.884_7
	$\Delta U_{\text{trans}}/(\epsilon/k_{\text{B}})$	0	-6.272_{12}	-2.915_{15}	-2.115_{14}	-2.666_{12}	-2.115_6	-0.755_4
1.01	$\Delta S_{\text{trans}}/(\epsilon/k_{\text{B}})$	6.973_8	8.374_{15}	7.624_{17}	7.182_{18}	7.178_{16}	7.182_9	6.651_9
	$\Delta A_{\text{trans}}/(\epsilon/k_{\text{B}})$	7.043_8	2.186_9	4.786_9	5.138_{11}	4.584_{10}	5.138_7	5.963_8
	$\Delta U_{\text{trans}}/(\epsilon/k_{\text{B}})$	0	-5.84_3	-2.681_{12}	-2.006_{14}	-2.492_5	-2.006_8	-0.7231_{15}
1.02	$\Delta S_{\text{trans}}/(\epsilon/k_{\text{B}})$	6.968_9	8.04_3	7.450_{16}	7.114_{16}	7.048_9	7.114_{13}	6.622_8
	$\Delta A_{\text{trans}}/(\epsilon/k_{\text{B}})$	7.107_9	2.356_9	4.918_{11}	5.250_9	4.698_8	5.250_{10}	6.031_8
	$\Delta U_{\text{trans}}/(\epsilon/k_{\text{B}})$	0	-5.34_3	-2.52_2	-1.844_{16}	-2.345_7	-1.844_{11}	-0.692_2
1.03	$\Delta S_{\text{trans}}/(\epsilon/k_{\text{B}})$	6.978_6	7.65_3	7.33_2	6.981_{18}	6.938_{12}	6.981_{14}	6.609_7
	$\Delta A_{\text{trans}}/(\epsilon/k_{\text{B}})$	7.188_6	2.535_{11}	5.029_8	5.346_{10}	4.801_{10}	5.346_9	6.115_7
	$\Delta U_{\text{trans}}/(\epsilon/k_{\text{B}})$	0	-4.899_{16}	-2.311_{10}	-1.740_{19}	-2.214_{10}	-1.740_9	-0.657_3
1.04	$\Delta S_{\text{trans}}/(\epsilon/k_{\text{B}})$	6.970_8	7.282_{19}	7.145_{13}	6.914_{19}	6.841_{12}	6.914_{12}	6.579_9
	$\Delta A_{\text{trans}}/(\epsilon/k_{\text{B}})$	7.249_8	2.674_{12}	5.120_9	5.450_7	4.901_8	5.450_9	6.185_8
	$\Delta U_{\text{trans}}/(\epsilon/k_{\text{B}})$	0	-4.54_4	-2.186_9	-1.655_9	-2.083_5	-1.655_{10}	-0.6254_{17}
1.05	$\Delta S_{\text{trans}}/(\epsilon/k_{\text{B}})$	6.983_8	7.00_3	7.083_{16}	6.863_{12}	6.743_{12}	6.863_{12}	6.559_7
	$\Delta A_{\text{trans}}/(\epsilon/k_{\text{B}})$	7.332_9	2.812_8	5.251_{14}	5.552_9	4.997_{11}	5.552_9	6.262_7
Eq. 5	$\Delta U_{\text{trans}}/(\epsilon/k_{\text{B}})$	0.03_7	-15.31_{11}	-6.85_6	-5.37_8	-6.11_8	4.84_8	1.91_7
	$\Delta S_{\text{trans}}/(\epsilon/k_{\text{B}})$	-2.78_3	-6.92_4	-4.61_3	-4.27_3	-4.24_3	-3.96_3	-3.12_3

Table 3.5: Internal energies, entropies, and Helmholtz energies of transfer for polymers from the solution phase to spherical pores for $N = 256$. Errors given are standard errors of the mean.

T/T_{LCCC}	Property	**A**	**B**	**AB**	**ABA**	**BAB**	**ABAB**	Alter
0.95	$\Delta U_{\mathrm{trans}}/(\epsilon/k_{\mathrm{B}})$	0	$-25.1_{1.5}$	-11.3_{7}	-10.2_{8}	-10.6_{5}	-9.1_{6}	-2.09_{11}
	$\Delta S_{\mathrm{trans}}/(\epsilon/k_{\mathrm{B}})$	-12.91_{4}	$-27.8_{1.6}$	-19.1_{8}	-18.9_{9}	-18.0_{6}	-17.5_{6}	-12.78_{12}
	$\Delta A_{\mathrm{trans}}/(\epsilon/k_{\mathrm{B}})$	12.26_{4}	1.37_{4}	6.79_{5}	7.70_{4}	6.45_{4}	7.50_{4}	10.05_{3}
0.96	$\Delta U_{\mathrm{trans}}/(\epsilon/k_{\mathrm{B}})$	0	$-22.2_{1.5}$	-10.2_{7}	-9.4_{9}	-9.8_{5}	-8.4_{6}	-1.92_{11}
	$\Delta S_{\mathrm{trans}}/(\epsilon/k_{\mathrm{B}})$	-12.88_{3}	$-25.1_{1.6}$	-18.0_{7}	-18.0_{9}	-17.1_{5}	-16.7_{6}	-12.74_{12}
	$\Delta A_{\mathrm{trans}}/(\epsilon/k_{\mathrm{B}})$	12.36_{3}	1.90_{5}	7.08_{4}	7.92_{5}	6.68_{4}	7.68_{4}	10.31_{3}
0.97	$\Delta U_{\mathrm{trans}}/(\epsilon/k_{\mathrm{B}})$	0	$-20.4_{1.7}$	-9.4_{6}	-8.6_{7}	-8.9_{6}	-7.7_{5}	-1.85_{10}
	$\Delta S_{\mathrm{trans}}/(\epsilon/k_{\mathrm{B}})$	-12.89_{4}	$-23.3_{1.7}$	-17.1_{7}	-17.2_{7}	-16.3_{6}	-16.1_{5}	-12.53_{11}
	$\Delta A_{\mathrm{trans}}/(\epsilon/k_{\mathrm{B}})$	12.50_{4}	2.27_{4}	7.26_{4}	8.13_{4}	6.95_{4}	7.94_{4}	10.31_{3}
0.98	$\Delta U_{\mathrm{trans}}/(\epsilon/k_{\mathrm{B}})$	0	$-18.1_{1.6}$	-8.5_{7}	-7.7_{7}	-8.0_{5}	-7.0_{5}	-1.73_{10}
	$\Delta S_{\mathrm{trans}}/(\epsilon/k_{\mathrm{B}})$	-12.88_{4}	$-21.1_{1.7}$	-16.4_{7}	-16.4_{7}	-15.6_{5}	-15.4_{5}	-12.43_{11}
	$\Delta A_{\mathrm{trans}}/(\epsilon/k_{\mathrm{B}})$	12.63_{4}	2.59_{4}	7.55_{4}	8.39_{4}	7.20_{4}	8.13_{4}	10.46_{3}
0.99	$\Delta U_{\mathrm{trans}}/(\epsilon/k_{\mathrm{B}})$	0	$-16.6_{1.5}$	-7.8_{6}	-6.8_{7}	-7.3_{5}	-6.3_{5}	-1.56_{12}
	$\Delta S_{\mathrm{trans}}/(\epsilon/k_{\mathrm{B}})$	-12.86_{5}	$-19.6_{1.6}$	-15.7_{6}	-15.7_{8}	-14.9_{5}	-14.8_{5}	-12.40_{12}
	$\Delta A_{\mathrm{trans}}/(\epsilon/k_{\mathrm{B}})$	12.73_{5}	2.84_{4}	7.72_{4}	8.67_{4}	7.44_{4}	8.35_{4}	10.72_{4}
1.00	$\Delta U_{\mathrm{trans}}/(\epsilon/k_{\mathrm{B}})$	0	$-14.1_{1.5}$	-7.0_{5}	-6.1_{7}	-6.6_{4}	-5.7_{4}	-1.50_{11}
	$\Delta S_{\mathrm{trans}}/(\epsilon/k_{\mathrm{B}})$	-12.93_{4}	$-17.4_{1.5}$	-14.9_{5}	-15.0_{7}	-14.2_{4}	-14.3_{4}	-12.28_{11}
	$\Delta A_{\mathrm{trans}}/(\epsilon/k_{\mathrm{B}})$	12.93_{4}	3.32_{4}	7.98_{4}	8.89_{4}	7.66_{4}	8.63_{3}	10.77_{4}
1.01	$\Delta U_{\mathrm{trans}}/(\epsilon/k_{\mathrm{B}})$	0	$-12.5_{1.7}$	-6.3_{6}	-5.7_{9}	-6.1_{6}	-5.2_{6}	-1.38_{14}
	$\Delta S_{\mathrm{trans}}/(\epsilon/k_{\mathrm{B}})$	-12.95_{4}	$-16.0_{1.7}$	-14.4_{5}	-14.7_{9}	-13.8_{6}	-13.9_{6}	-12.21_{14}
	$\Delta A_{\mathrm{trans}}/(\epsilon/k_{\mathrm{B}})$	13.08_{4}	3.67_{4}	8.18_{4}	9.10_{4}	7.84_{4}	8.83_{4}	10.95_{4}
1.02	$\Delta U_{\mathrm{trans}}/(\epsilon/k_{\mathrm{B}})$	0	$-11.4_{1.7}$	-5.6_{5}	-5.1_{8}	-5.3_{6}	-4.7_{6}	-1.29_{13}
	$\Delta S_{\mathrm{trans}}/(\epsilon/k_{\mathrm{B}})$	-12.94_{4}	$-14.9_{1.6}$	-13.8_{5}	-14.0_{8}	-13.2_{5}	-13.4_{6}	-12.08_{14}
	$\Delta A_{\mathrm{trans}}/(\epsilon/k_{\mathrm{B}})$	13.20_{4}	3.87_{4}	8.44_{4}	9.19_{4}	8.13_{4}	8.98_{4}	11.03_{4}
1.03	$\Delta U_{\mathrm{trans}}/(\epsilon/k_{\mathrm{B}})$	0	$-10.2_{1.5}$	-5.0_{4}	-4.5_{8}	-4.8_{6}	-4.1_{5}	-1.18_{11}
	$\Delta S_{\mathrm{trans}}/(\epsilon/k_{\mathrm{B}})$	-12.96_{4}	$-13.9_{1.5}$	-13.3_{4}	-13.6_{8}	-12.8_{6}	-13.0_{5}	-12.03_{12}
	$\Delta A_{\mathrm{trans}}/(\epsilon/k_{\mathrm{B}})$	13.34_{4}	4.14_{4}	8.68_{4}	9.52_{4}	8.34_{5}	9.24_{4}	11.21_{4}
1.04	$\Delta U_{\mathrm{trans}}/(\epsilon/k_{\mathrm{B}})$	0	$-8.6_{1.2}$	-4.4_{5}	-4.1_{7}	-4.3_{6}	-3.8_{5}	-1.08_{14}
	$\Delta S_{\mathrm{trans}}/(\epsilon/k_{\mathrm{B}})$	-12.93_{4}	$-12.6_{1.1}$	-12.8_{5}	-13.3_{7}	-12.3_{6}	-12.8_{5}	-12.05_{14}
	$\Delta A_{\mathrm{trans}}/(\epsilon/k_{\mathrm{B}})$	13.45_{4}	4.57_{4}	8.92_{5}	9.78_{4}	8.56_{4}	9.44_{3}	11.46_{4}
1.05	$\Delta U_{\mathrm{trans}}/(\epsilon/k_{\mathrm{B}})$	0	$-7.6_{1.1}$	-4.1_{4}	-3.7_{7}	-4.0_{4}	-3.3_{5}	-1.01_{12}
	$\Delta S_{\mathrm{trans}}/(\epsilon/k_{\mathrm{B}})$	-12.91_{4}	$-11.8_{1.0}$	-12.5_{4}	-12.9_{7}	-12.0_{4}	-12.3_{5}	-11.92_{12}
	$\Delta A_{\mathrm{trans}}/(\epsilon/k_{\mathrm{B}})$	13.56_{4}	4.79_{5}	9.06_{4}	9.85_{5}	8.63_{4}	9.65_{4}	11.51_{4}
Eq 3.5	$\Delta U_{\mathrm{trans}}/(\epsilon/k_{\mathrm{B}})$	$0.9_{1.0}$	$-57.1_{1.2}$	$-26.7_{1.2}$	$-25.5_{1.2}$	$-25.6_{1.0}$	$-21.8_{1.0}$	-6.1_{8}
	$\Delta S_{\mathrm{trans}}/(\epsilon/k_{\mathrm{B}})$	-6.7_{4}	-23.5_{5}	-14.6_{5}	-14.8_{5}	-14.0_{4}	-13.1_{4}	-8.3_{3}

Table 3.6: Internal energies, entropies, and Helmholtz energies of transfer for polymers from the solution phase to cylindrical pores for $N = 32$. Errors designate standard errors of the mean.

T	Property	**A**	**B**	**AB**	**ABA**	**BAB**	**ABAB**	Alter
	$\Delta U_{\text{trans}}/(\epsilon/k_{\text{B}})$	0	-1.8416_{18}	-0.5482_{4}	-0.3912_{6}	-0.4986_{6}	-0.3886_{7}	-0.2389_{3}
0.95	$\Delta S_{\text{trans}}/(\epsilon/k_{\text{B}})$	1.6946_{14}	2.151_{2}	1.7147_{17}	1.6858_{16}	1.6218_{10}	1.6393_{16}	1.5703_{14}
	$\Delta A_{\text{trans}}/(\epsilon/k_{\text{B}})$	1.6098_{13}	0.2016_{14}	1.0808_{16}	1.2103_{14}	1.0421_{7}	1.1687_{13}	1.2529_{13}
	$\Delta U_{\text{trans}}/(\epsilon/k_{\text{B}})$	0	-1.778_{2}	-0.5349_{8}	-0.3813_{8}	-0.4888_{5}	-0.3813_{4}	-0.2356_{4}
0.96	$\Delta S_{\text{trans}}/(\epsilon/k_{\text{B}})$	1.6946_{13}	2.108_{3}	1.711_{2}	1.6340_{13}	1.6165_{17}	1.6340_{17}	1.570_{2}
	$\Delta A_{\text{trans}}/(\epsilon/k_{\text{B}})$	1.6268_{12}	0.2461_{17}	1.1079_{19}	1.1873_{9}	1.0631_{16}	1.1873_{16}	1.272_{2}
	$\Delta U_{\text{trans}}/(\epsilon/k_{\text{B}})$	0	-1.7192_{19}	-0.5204_{6}	-0.3738_{6}	-0.4787_{6}	-0.3738_{6}	-0.2323_{3}
0.97	$\Delta S_{\text{trans}}/(\epsilon/k_{\text{B}})$	1.6965_{11}	2.068_{2}	1.702_{3}	1.6306_{14}	1.6137_{10}	1.6306_{18}	1.5704_{19}
	$\Delta A_{\text{trans}}/(\epsilon/k_{\text{B}})$	1.6456_{11}	0.2865_{14}	1.130_{3}	1.2079_{13}	1.0866_{8}	1.2079_{16}	1.2910_{18}
	$\Delta U_{\text{trans}}/(\epsilon/k_{\text{B}})$	0	-1.6661_{13}	-0.5092_{7}	-0.3665_{2}	-0.4696_{5}	-0.3665_{5}	-0.2290_{3}
0.98	$\Delta S_{\text{trans}}/(\epsilon/k_{\text{B}})$	1.6966_{13}	2.0320_{16}	1.6969_{18}	1.6296_{14}	1.6095_{12}	1.6296_{14}	1.5703_{17}
	$\Delta A_{\text{trans}}/(\epsilon/k_{\text{B}})$	1.6627_{13}	0.3253_{7}	1.1538_{16}	1.2306_{13}	1.1077_{11}	1.2306_{13}	1.3099_{17}
	$\Delta U_{\text{trans}}/(\epsilon/k_{\text{B}})$	0	-1.6086_{14}	-0.4970_{7}	-0.3608_{6}	-0.4623_{5}	-0.3608_{4}	-0.2258_{3}
0.99	$\Delta S_{\text{trans}}/(\epsilon/k_{\text{B}})$	1.6971_{7}	1.993_{2}	1.6900_{15}	1.6277_{18}	1.6074_{11}	1.6277_{19}	1.5711_{16}
	$\Delta A_{\text{trans}}/(\epsilon/k_{\text{B}})$	1.6801_{7}	0.3645_{17}	1.1761_{13}	1.2506_{17}	1.1290_{10}	1.2506_{18}	1.3296_{16}
	$\Delta U_{\text{trans}}/(\epsilon/k_{\text{B}})$	0	-1.5620_{14}	-0.4865_{8}	-0.3537_{5}	-0.4532_{4}	-0.3537_{4}	-0.2229_{2}
1.00	$\Delta S_{\text{trans}}/(\epsilon/k_{\text{B}})$	1.6958_{17}	1.965_{3}	1.6854_{17}	1.6198_{16}	1.6070_{18}	1.6198_{15}	1.5692_{14}
	$\Delta A_{\text{trans}}/(\epsilon/k_{\text{B}})$	1.6958_{17}	0.403_{2}	1.1990_{14}	1.2661_{15}	1.1538_{17}	1.2661_{14}	1.3463_{14}
	$\Delta U_{\text{trans}}/(\epsilon/k_{\text{B}})$	0	-1.5127_{9}	-0.4749_{9}	-0.3468_{6}	-0.4453_{4}	-0.3468_{6}	-0.2202_{3}
1.01	$\Delta S_{\text{trans}}/(\epsilon/k_{\text{B}})$	1.6952_{12}	1.9312_{13}	1.6804_{13}	1.6247_{18}	1.6056_{13}	1.625_{2}	1.573_{2}
	$\Delta A_{\text{trans}}/(\epsilon/k_{\text{B}})$	1.7121_{12}	0.4378_{9}	1.2223_{10}	1.2941_{17}	1.1763_{12}	1.294_{2}	1.368_{2}
	$\Delta U_{\text{trans}}/(\epsilon/k_{\text{B}})$	0	-1.4687_{12}	-0.4642_{10}	-0.3408_{5}	-0.4376_{5}	-0.3408_{2}	-0.2176_{2}
1.02	$\Delta S_{\text{trans}}/(\epsilon/k_{\text{B}})$	1.6929_{10}	1.904_{2}	1.6755_{18}	1.6249_{11}	1.6008_{12}	1.6249_{10}	1.5758_{15}
	$\Delta A_{\text{trans}}/(\epsilon/k_{\text{B}})$	1.7268_{10}	0.473_{2}	1.2448_{15}	1.3166_{10}	1.1952_{11}	1.3166_{10}	1.3898_{15}
	$\Delta U_{\text{trans}}/(\epsilon/k_{\text{B}})$	0	-1.4263_{10}	-0.4536_{5}	-0.3348_{4}	-0.4300_{8}	-0.3348_{3}	-0.2146_{2}
1.03	$\Delta S_{\text{trans}}/(\epsilon/k_{\text{B}})$	1.6933_{14}	1.8775_{11}	1.6661_{12}	1.6213_{14}	1.5984_{18}	1.6213_{15}	1.5750_{15}
	$\Delta A_{\text{trans}}/(\epsilon/k_{\text{B}})$	1.7441_{15}	0.5075_{5}	1.2625_{11}	1.3351_{14}	1.2164_{17}	1.3351_{15}	1.4077_{16}
	$\Delta U_{\text{trans}}/(\epsilon/k_{\text{B}})$	0	-1.3855_{11}	-0.4445_{8}	-0.3289_{5}	-0.4222_{6}	-0.3289_{5}	-0.2122_{3}
1.04	$\Delta S_{\text{trans}}/(\epsilon/k_{\text{B}})$	1.6948_{13}	1.8550_{16}	1.6663_{18}	1.6193_{12}	1.5940_{14}	1.6193_{19}	1.5731_{12}
	$\Delta A_{\text{trans}}/(\epsilon/k_{\text{B}})$	1.7626_{13}	0.5437_{12}	1.2885_{17}	1.3552_{11}	1.2356_{13}	1.3552_{19}	1.4238_{13}
	$\Delta U_{\text{trans}}/(\epsilon/k_{\text{B}})$	0	-1.3470_{11}	-0.4353_{7}	-0.3233_{3}	-0.4155_{5}	-0.3233_{6}	-0.2101_{4}
1.05	$\Delta S_{\text{trans}}/(\epsilon/k_{\text{B}})$	1.6936_{13}	1.835_{2}	1.6634_{17}	1.6172_{18}	1.593_{2}	1.617_{2}	1.5740_{14}
	$\Delta A_{\text{trans}}/(\epsilon/k_{\text{B}})$	1.7782_{13}	0.5803_{18}	1.3113_{16}	1.3748_{18}	1.257_{2}	1.375_{2}	1.4426_{15}
Eq. 5	$\Delta U_{\text{trans}}/(\epsilon/k_{\text{B}})$	0.020_{12}	-3.40_{2}	-1.077_{17}	-0.848_{13}	-1.012_{14}	-0.8818_{16}	-0.565_{16}
	$\Delta S_{\text{trans}}/(\epsilon/k_{\text{B}})$	-0.667_{5}	-1.499_{8}	-0.910_{7}	-0.868_{5}	-0.865_{5}	-0.836_{7}	-0.766_{6}

Table 3.7: Internal energies, entropies, and Helmholtz energies of transfer for polymers from the solution phase to cylindrical pores for $N = 64$. Errors designate standard errors of the mean.

T	Property	**A**	**B**	**AB**	**ABA**	**BAB**	**ABAB**	Alter
	$\Delta U_{\mathrm{trans}}/(\epsilon/k_{\mathrm{B}})$	0	-3.610_6	-1.218_2	-0.841_2	-1.001_4	-0.8109_{18}	-0.3606_7
0.95	$\Delta S_{\mathrm{trans}}/(\epsilon/k_{\mathrm{B}})$	2.426_2	3.805_8	2.755_3	2.626_4	2.480_7	2.514_3	2.295_3
	$\Delta A_{\mathrm{trans}}/(\epsilon/k_{\mathrm{B}})$	2.305_2	0.005_5	1.399_2	1.653_3	1.356_5	1.578_3	1.820_3
	$\Delta U_{\mathrm{trans}}/(\epsilon/k_{\mathrm{B}})$	0	-3.406_5	-1.159_2	-0.7833_{14}	-0.9656_{19}	-0.7833_{10}	-0.3517_5
0.96	$\Delta S_{\mathrm{trans}}/(\epsilon/k_{\mathrm{B}})$	2.428_4	3.642_6	2.712_4	2.491_3	2.458_4	2.491_2	2.293_5
	$\Delta A_{\mathrm{trans}}/(\epsilon/k_{\mathrm{B}})$	2.331_4	0.090_3	1.444_3	1.608_2	1.394_3	1.608_2	1.849_4
	$\Delta U_{\mathrm{trans}}/(\epsilon/k_{\mathrm{B}})$	0	-3.236_5	-1.117_2	-0.751_3	-0.9332_{14}	-0.751_2	-0.3430_9
0.97	$\Delta S_{\mathrm{trans}}/(\epsilon/k_{\mathrm{B}})$	2.426_3	3.500_6	2.679_3	2.470_5	2.435_4	2.470_4	2.283_3
	$\Delta A_{\mathrm{trans}}/(\epsilon/k_{\mathrm{B}})$	2.353_3	0.159_4	1.481_3	1.645_4	1.429_4	1.645_3	1.871_3
	$\Delta U_{\mathrm{trans}}/(\epsilon/k_{\mathrm{B}})$	0	-3.058_4	-1.0670_{11}	-0.7235_{17}	-0.8974_{12}	-0.723_3	-0.3338_7
0.98	$\Delta S_{\mathrm{trans}}/(\epsilon/k_{\mathrm{B}})$	2.429_2	3.365_4	2.640_3	2.453_3	2.415_3	2.453_4	2.284_3
	$\Delta A_{\mathrm{trans}}/(\epsilon/k_{\mathrm{B}})$	2.380_2	0.239_2	1.520_3	1.681_3	1.469_3	1.681_3	1.904_3
	$\Delta U_{\mathrm{trans}}/(\epsilon/k_{\mathrm{B}})$	0	-2.904_6	-1.027_3	-0.7041_{10}	-0.8678_{11}	-0.7041_{19}	-0.3253_5
0.99	$\Delta S_{\mathrm{trans}}/(\epsilon/k_{\mathrm{B}})$	2.430_2	3.238_7	2.616_6	2.436_3	2.397_3	2.436_4	2.280_3
	$\Delta A_{\mathrm{trans}}/(\epsilon/k_{\mathrm{B}})$	2.406_2	0.302_4	1.563_5	1.708_3	1.505_3	1.708_3	1.932_3
	$\Delta U_{\mathrm{trans}}/(\epsilon/k_{\mathrm{B}})$	0	-2.761_5	-0.9825_{15}	-0.676_2	-0.8379_{13}	-0.676_2	-0.3185_5
1.00	$\Delta S_{\mathrm{trans}}/(\epsilon/k_{\mathrm{B}})$	2.428_2	3.129_7	2.581_3	2.417_4	2.376_3	2.417_3	2.277_4
	$\Delta A_{\mathrm{trans}}/(\epsilon/k_{\mathrm{B}})$	2.428_2	0.368_4	1.599_3	1.740_3	1.538_2	1.740_3	1.959_4
	$\Delta U_{\mathrm{trans}}/(\epsilon/k_{\mathrm{B}})$	0	-2.618_3	-0.9429_{19}	-0.6550_{15}	-0.8104_{15}	-0.6550_{12}	-0.3098_7
1.01	$\Delta S_{\mathrm{trans}}/(\epsilon/k_{\mathrm{B}})$	2.428_2	3.023_3	2.554_4	2.404_2	2.358_4	2.404_4	2.276_3
	$\Delta A_{\mathrm{trans}}/(\epsilon/k_{\mathrm{B}})$	2.453_2	0.4352_{15}	1.637_3	1.7730_{15}	1.571_3	1.773_3	1.989_3
	$\Delta U_{\mathrm{trans}}/(\epsilon/k_{\mathrm{B}})$	0	-2.502_4	-0.912_2	-0.6309_{15}	-0.7842_{11}	-0.6309_{18}	-0.3039_7
1.02	$\Delta S_{\mathrm{trans}}/(\epsilon/k_{\mathrm{B}})$	2.425_3	2.944_5	2.532_3	2.387_5	2.352_3	2.387_3	2.268_3
	$\Delta A_{\mathrm{trans}}/(\epsilon/k_{\mathrm{B}})$	2.473_3	0.501_3	1.671_2	1.804_4	1.615_2	1.804_3	2.009_3
	$\Delta U_{\mathrm{trans}}/(\epsilon/k_{\mathrm{B}})$	0	-2.378_4	-0.873_2	-0.614_2	-0.7602_{11}	-0.6138_{10}	-0.2966_5
1.03	$\Delta S_{\mathrm{trans}}/(\epsilon/k_{\mathrm{B}})$	2.424_3	2.857_5	2.507_5	2.380_3	2.330_3	2.380_3	2.265_3
	$\Delta A_{\mathrm{trans}}/(\epsilon/k_{\mathrm{B}})$	2.497_3	0.564_3	1.709_5	1.838_3	1.640_3	1.838_3	2.037_3
	$\Delta U_{\mathrm{trans}}/(\epsilon/k_{\mathrm{B}})$	0	-2.268_4	-0.843_3	-0.593_2	-0.7372_{13}	-0.5925_{12}	-0.2901_6
1.04	$\Delta S_{\mathrm{trans}}/(\epsilon/k_{\mathrm{B}})$	2.427_4	2.776_4	2.489_5	2.372_3	2.321_2	2.372_2	2.264_2
	$\Delta A_{\mathrm{trans}}/(\epsilon/k_{\mathrm{B}})$	2.524_4	0.6194_{19}	1.746_4	1.8745_{19}	1.677_2	1.875_2	2.064_2
	$\Delta U_{\mathrm{trans}}/(\epsilon/k_{\mathrm{B}})$	0	-2.173_5	-0.811_2	-0.5741_{15}	-0.7122_8	-0.5741_{11}	-0.2838_8
1.05	$\Delta S_{\mathrm{trans}}/(\epsilon/k_{\mathrm{B}})$	2.425_4	2.712_8	2.473_2	2.365_4	2.312_3	2.365_3	2.267_3
	$\Delta A_{\mathrm{trans}}/(\epsilon/k_{\mathrm{B}})$	2.546_4	0.675_7	1.7862_{17}	1.909_4	1.716_3	1.909_3	2.097_3
Eq. 5	$\Delta U_{\mathrm{trans}}/(\epsilon/k_{\mathrm{B}})$	0.02_3	-6.33_5	-2.23_3	-1.64_3	-2.03_3	-1.55_3	-0.78_3
	$\Delta S_{\mathrm{trans}}/(\epsilon/k_{\mathrm{B}})$	-0.961_{11}	-2.68_2	-1.530_{12}	-1.386_{12}	-1.426_{12}	-1.315_{11}	-1.094_{12}

Table 3.8: Internal energies, entropies, and Helmholtz energies of transfer for polymers from the solution phase to cylindrical pores for $N = 128$. Errors designate standard errors of the mean.

T	Property	**A**	**B**	**AB**	**ABA**	**BAB**	**ABAB**	Alter
	$\Delta U_{\text{trans}}/(\epsilon/k_{\text{B}})$	0	-8.12_{3}	-3.005_{15}	-2.43_{2}	-2.428_{10}	-2.228_{6}	-0.57_{3}
0.95	$\Delta S_{\text{trans}}/(\epsilon/k_{\text{B}})$	3.850_{15}	8.27_{4}	5.222_{18}	5.09_{2}	4.574_{16}	4.772_{11}	3.71_{8}
	$\Delta A_{\text{trans}}/(\epsilon/k_{\text{B}})$	3.658_{14}	-0.258_{11}	1.956_{8}	2.408_{12}	1.918_{11}	2.306_{9}	2.96_{7}
	$\Delta U_{\text{trans}}/(\epsilon/k_{\text{B}})$	0	-7.48_{4}	-2.815_{17}	-2.102_{17}	-2.295_{3}	-2.102_{8}	-0.55_{3}
0.96	$\Delta S_{\text{trans}}/(\epsilon/k_{\text{B}})$	3.855_{13}	7.68_{5}	5.05_{2}	4.66_{2}	4.455_{8}	4.664_{12}	3.69_{13}
	$\Delta A_{\text{trans}}/(\epsilon/k_{\text{B}})$	3.701_{12}	-0.105_{14}	2.030_{16}	2.375_{13}	1.982_{7}	2.375_{8}	2.99_{12}
	$\Delta U_{\text{trans}}/(\epsilon/k_{\text{B}})$	0	-6.92_{4}	-2.642_{14}	-2.008_{13}	-2.166_{14}	-2.008_{9}	-0.5296_{17}
0.97	$\Delta S_{\text{trans}}/(\epsilon/k_{\text{B}})$	3.853_{12}	7.18_{4}	4.906_{17}	4.579_{18}	4.368_{18}	4.579_{13}	3.676_{7}
	$\Delta A_{\text{trans}}/(\epsilon/k_{\text{B}})$	3.737_{12}	0.053_{11}	2.117_{9}	2.434_{11}	2.071_{11}	2.434_{9}	3.036_{7}
	$\Delta U_{\text{trans}}/(\epsilon/k_{\text{B}})$	0	-6.48_{3}	-2.462_{14}	-1.896_{11}	-2.057_{6}	-1.896_{6}	-0.515_{2}
0.98	$\Delta S_{\text{trans}}/(\epsilon/k_{\text{B}})$	3.856_{11}	6.77_{3}	4.764_{18}	4.485_{16}	4.274_{7}	4.485_{14}	3.652_{12}
	$\Delta A_{\text{trans}}/(\epsilon/k_{\text{B}})$	3.779_{11}	0.158_{12}	2.207_{11}	2.499_{10}	2.131_{4}	2.499_{13}	3.064_{12}
	$\Delta U_{\text{trans}}/(\epsilon/k_{\text{B}})$	0	-5.966_{17}	-2.324_{14}	-1.791_{15}	-1.953_{10}	-1.791_{9}	-0.4937_{12}
0.99	$\Delta S_{\text{trans}}/(\epsilon/k_{\text{B}})$	3.858_{10}	6.32_{2}	4.633_{17}	4.392_{17}	4.185_{16}	4.392_{15}	3.643_{5}
	$\Delta A_{\text{trans}}/(\epsilon/k_{\text{B}})$	3.819_{10}	0.293_{11}	2.263_{9}	2.557_{8}	2.190_{13}	2.557_{12}	3.113_{5}
	$\Delta U_{\text{trans}}/(\epsilon/k_{\text{B}})$	0	-5.56_{2}	-2.203_{12}	-1.692_{16}	-1.837_{6}	-1.692_{8}	-0.473_{2}
1.00	$\Delta S_{\text{trans}}/(\epsilon/k_{\text{B}})$	3.849_{15}	6.00_{3}	4.551_{19}	4.29_{2}	4.095_{9}	4.295_{13}	3.640_{12}
	$\Delta A_{\text{trans}}/(\epsilon/k_{\text{B}})$	3.849_{15}	0.441_{15}	2.349_{15}	2.603_{12}	2.258_{7}	2.603_{10}	3.168_{12}
	$\Delta U_{\text{trans}}/(\epsilon/k_{\text{B}})$	0	-5.152_{19}	-2.047_{7}	-1.619_{7}	-1.762_{6}	-1.619_{9}	-0.458_{2}
1.01	$\Delta S_{\text{trans}}/(\epsilon/k_{\text{B}})$	3.846_{5}	5.65_{2}	4.423_{11}	4.249_{14}	4.029_{10}	4.249_{14}	3.631_{14}
	$\Delta A_{\text{trans}}/(\epsilon/k_{\text{B}})$	3.885_{5}	0.556_{10}	2.420_{8}	2.673_{12}	2.308_{8}	2.673_{12}	3.208_{14}
	$\Delta U_{\text{trans}}/(\epsilon/k_{\text{B}})$	0	-4.79_{2}	-1.930_{10}	-1.532_{8}	-1.655_{6}	-1.532_{7}	-0.4413_{10}
1.02	$\Delta S_{\text{trans}}/(\epsilon/k_{\text{B}})$	3.875_{12}	5.35_{3}	4.325_{15}	4.176_{12}	3.966_{12}	4.176_{13}	3.630_{9}
	$\Delta A_{\text{trans}}/(\epsilon/k_{\text{B}})$	3.953_{13}	0.662_{11}	2.482_{12}	2.728_{9}	2.390_{10}	2.728_{11}	3.262_{9}
	$\Delta U_{\text{trans}}/(\epsilon/k_{\text{B}})$	0	-4.491_{12}	-1.817_{6}	-1.436_{11}	-1.585_{7}	-1.436_{8}	-0.426_{3}
1.03	$\Delta S_{\text{trans}}/(\epsilon/k_{\text{B}})$	3.852_{10}	5.106_{14}	4.260_{9}	-1.394_{13}	3.908_{13}	4.122_{16}	3.605_{13}
	$\Delta A_{\text{trans}}/(\epsilon/k_{\text{B}})$	3.968_{10}	0.768_{7}	2.571_{6}	2.810_{9}	2.441_{11}	2.810_{15}	3.287_{13}
	$\Delta U_{\text{trans}}/(\epsilon/k_{\text{B}})$	0	-4.21_{2}	-1.722_{5}	-1.383_{7}	-1.502_{7}	-1.383_{7}	-0.414_{2}
1.04	$\Delta S_{\text{trans}}/(\epsilon/k_{\text{B}})$	3.844_{14}	4.89_{3}	4.172_{7}	-1.330_{10}	3.852_{12}	4.064_{12}	3.606_{15}
	$\Delta A_{\text{trans}}/(\epsilon/k_{\text{B}})$	3.998_{15}	0.873_{17}	2.616_{5}	2.843_{7}	2.504_{10}	2.843_{10}	3.336_{15}
	$\Delta U_{\text{trans}}/(\epsilon/k_{\text{B}})$	0	-3.862_{15}	-1.629_{13}	-1.306_{10}	-1.428_{9}	-1.306_{5}	-0.4001_{12}
1.05	$\Delta S_{\text{trans}}/(\epsilon/k_{\text{B}})$	3.845_{14}	4.63_{2}	4.100_{19}	4.026_{13}	3.813_{13}	4.026_{14}	3.583_{6}
	$\Delta A_{\text{trans}}/(\epsilon/k_{\text{B}})$	4.038_{17}	1.000_{14}	2.676_{15}	2.922_{9}	2.576_{10}	2.922_{13}	3.362_{6}
Eq. 5	$\Delta U_{\text{trans}}/(\epsilon/k_{\text{B}})$	0.03_{4}	-12.01_{5}	-4.97_{4}	-3.73_{4}	-4.23_{4}	-3.43_{4}	-1.05_{4}
	$\Delta S_{\text{trans}}/(\epsilon/k_{\text{B}})$	-1.53_{5}	-4.97_{6}	-2.92_{4}	-2.60_{4}	-2.60_{4}	-2.42_{4}	-1.69_{4}

Table 3.9: Internal energies, entropies, and Helmholtz energies of transfer for polymers from the solution phase to cylindrical pores for $N = 256$. All errors are given as standard error of the mean.

T/T_{LCCC}	Property	**A**	**B**	**AB**	**ABA**	**BAB**	**ABAB**	Alter
0.95	$\Delta U_{\mathrm{trans}}/(\epsilon/k_{\mathrm{B}})$	0	-18.2_{3}	-7.58_{13}	-6.16_{14}	-6.99_{8}	-5.74_{9}	-1.184_{18}
	$\Delta S_{\mathrm{trans}}/(\epsilon/k_{\mathrm{B}})$	-7.08_{4}	-18.7_{3}	-11.36_{14}	-10.49_{16}	-10.57_{10}	-9.93_{11}	-6.98_{4}
	$\Delta A_{\mathrm{trans}}/(\epsilon/k_{\mathrm{B}})$	6.73_{3}	-0.51_{5}	3.22_{5}	3.80_{5}	3.05_{4}	3.70_{4}	5.45_{3}
0.96	$\Delta U_{\mathrm{trans}}/(\epsilon/k_{\mathrm{B}})$	0	-16.9_{2}	-7.09_{13}	-5.60_{14}	-6.42_{8}	-5.23_{8}	-1.130_{16}
	$\Delta S_{\mathrm{trans}}/(\epsilon/k_{\mathrm{B}})$	-7.13_{4}	-17.3_{2}	-10.88_{14}	-9.95_{16}	-10.05_{9}	-9.46_{9}	-6.93_{3}
	$\Delta A_{\mathrm{trans}}/(\epsilon/k_{\mathrm{B}})$	6.85_{4}	-0.29_{4}	3.36_{4}	3.95_{5}	3.23_{4}	3.86_{4}	5.52_{3}
0.97	$\Delta U_{\mathrm{trans}}/(\epsilon/k_{\mathrm{B}})$	0	-15.5_{2}	-6.42_{12}	-5.09_{13}	-6.01_{7}	-4.83_{9}	-1.063_{16}
	$\Delta S_{\mathrm{trans}}/(\epsilon/k_{\mathrm{B}})$	-7.14_{4}	-15.9_{2}	-10.22_{13}	-9.49_{15}	-9.62_{9}	-9.14_{10}	-6.89_{4}
	$\Delta A_{\mathrm{trans}}/(\epsilon/k_{\mathrm{B}})$	6.92_{4}	-0.11_{5}	3.49_{5}	4.12_{5}	3.32_{4}	4.04_{5}	5.62_{3}
0.98	$\Delta U_{\mathrm{trans}}/(\epsilon/k_{\mathrm{B}})$	0	-13.8_{2}	-5.86_{12}	-4.60_{13}	-5.51_{7}	-4.44_{7}	-1.019_{14}
	$\Delta S_{\mathrm{trans}}/(\epsilon/k_{\mathrm{B}})$	-7.07_{4}	-14.3_{2}	-9.74_{13}	-9.12_{14}	-9.23_{8}	-8.80_{8}	-6.81_{4}
	$\Delta A_{\mathrm{trans}}/(\epsilon/k_{\mathrm{B}})$	6.93_{4}	0.26_{4}	3.69_{6}	4.33_{5}	3.54_{4}	4.19_{4}	5.65_{3}
0.99	$\Delta U_{\mathrm{trans}}/(\epsilon/k_{\mathrm{B}})$	0	-12.7_{3}	-5.65_{16}	-4.59_{19}	-5.19_{11}	-4.15_{8}	-0.975_{14}
	$\Delta S_{\mathrm{trans}}/(\epsilon/k_{\mathrm{B}})$	-6.98_{5}	-13.3_{3}	-9.43_{18}	-8.95_{21}	-8.86_{12}	-8.47_{9}	-6.75_{5}
	$\Delta A_{\mathrm{trans}}/(\epsilon/k_{\mathrm{B}})$	6.91_{5}	0.46_{5}	3.68_{8}	4.27_{8}	3.58_{5}	4.24_{4}	5.71_{4}
1.00	$\Delta U_{\mathrm{trans}}/(\epsilon/k_{\mathrm{B}})$	0	-11.4_{2}	-5.00_{9}	-3.81_{12}	-4.73_{7}	-3.82_{8}	-0.938_{16}
	$\Delta S_{\mathrm{trans}}/(\epsilon/k_{\mathrm{B}})$	-7.05_{3}	-12.1_{2}	-8.96_{10}	-8.42_{13}	-8.51_{8}	-8.20_{9}	-6.74_{4}
	$\Delta A_{\mathrm{trans}}/(\epsilon/k_{\mathrm{B}})$	7.05_{3}	0.69_{4}	3.96_{4}	4.61_{5}	3.78_{4}	4.38_{4}	5.80_{3}
1.01	$\Delta U_{\mathrm{trans}}/(\epsilon/k_{\mathrm{B}})$	0	-10.4_{2}	-4.55_{8}	-3.48_{11}	-4.35_{6}	-3.44_{7}	-0.867_{15}
	$\Delta S_{\mathrm{trans}}/(\epsilon/k_{\mathrm{B}})$	-7.06_{5}	-11.2_{2}	-8.55_{9}	-8.16_{12}	-8.18_{7}	-7.97_{8}	-6.75_{4}
	$\Delta A_{\mathrm{trans}}/(\epsilon/k_{\mathrm{B}})$	7.13_{5}	0.86_{5}	4.08_{4}	4.76_{5}	3.92_{4}	4.61_{4}	5.95_{4}
1.02	$\Delta U_{\mathrm{trans}}/(\epsilon/k_{\mathrm{B}})$	0	-9.5_{2}	-4.10_{8}	-3.16_{9}	-3.94_{6}	-3.23_{6}	-0.840_{11}
	$\Delta S_{\mathrm{trans}}/(\epsilon/k_{\mathrm{B}})$	-6.95_{4}	-10.3_{2}	-8.21_{10}	-7.88_{10}	-7.91_{7}	-7.76_{8}	-6.70_{4}
	$\Delta A_{\mathrm{trans}}/(\epsilon/k_{\mathrm{B}})$	7.09_{4}	1.10_{5}	4.28_{5}	4.88_{5}	4.13_{4}	4.68_{5}	5.99_{3}
1.03	$\Delta U_{\mathrm{trans}}/(\epsilon/k_{\mathrm{B}})$	0	-8.21_{18}	-3.80_{9}	-2.86_{8}	-3.70_{5}	-2.97_{6}	-0.790_{12}
	$\Delta S_{\mathrm{trans}}/(\epsilon/k_{\mathrm{B}})$	-7.03_{5}	-9.39_{18}	-7.98_{10}	-7.66_{9}	-7.67_{6}	-7.54_{7}	-6.65_{4}
	$\Delta A_{\mathrm{trans}}/(\epsilon/k_{\mathrm{B}})$	7.24_{5}	1.46_{5}	4.41_{5}	5.03_{5}	4.19_{4}	4.80_{4}	6.06_{4}
1.04	$\Delta U_{\mathrm{trans}}/(\epsilon/k_{\mathrm{B}})$	0	-7.53_{18}	-3.47_{8}	-2.71_{9}	-3.38_{6}	-2.75_{6}	-0.747_{14}
	$\Delta S_{\mathrm{trans}}/(\epsilon/k_{\mathrm{B}})$	-7.06_{4}	-8.82_{18}	-7.68_{9}	-7.55_{9}	-7.43_{7}	-7.35_{7}	-6.68_{4}
	$\Delta A_{\mathrm{trans}}/(\epsilon/k_{\mathrm{B}})$	7.35_{4}	1.64_{5}	4.52_{5}	5.14_{4}	4.34_{4}	4.90_{5}	6.20_{4}
1.05	$\Delta U_{\mathrm{trans}}/(\epsilon/k_{\mathrm{B}})$	0	-6.93_{17}	-3.19_{7}	-2.42_{7}	-3.19_{6}	-2.53_{5}	-0.711_{12}
	$\Delta S_{\mathrm{trans}}/(\epsilon/k_{\mathrm{B}})$	-7.16_{5}	-8.28_{16}	-7.45_{8}	-7.27_{8}	-7.24_{8}	-7.18_{6}	-6.66_{12}
	$\Delta A_{\mathrm{trans}}/(\epsilon/k_{\mathrm{B}})$	7.52_{5}	1.76_{5}	4.63_{4}	5.22_{4}	4.41_{5}	5.01_{3}	6.28_{4}
Eq 3.5	$\Delta U_{\mathrm{trans}}/(\epsilon/k_{\mathrm{B}})$	0.4_{4}	-22.8_{5}	-10.7_{5}	-10.2_{5}	-10.2_{4}	-8.7_{4}	-2.5_{3}
	$\Delta S_{\mathrm{trans}}/(\epsilon/k_{\mathrm{B}})$	-2.69_{16}	-9.40_{18}	-5.84_{19}	-5.9_{2}	-5.60_{16}	-5.25_{16}	-3.32_{13}

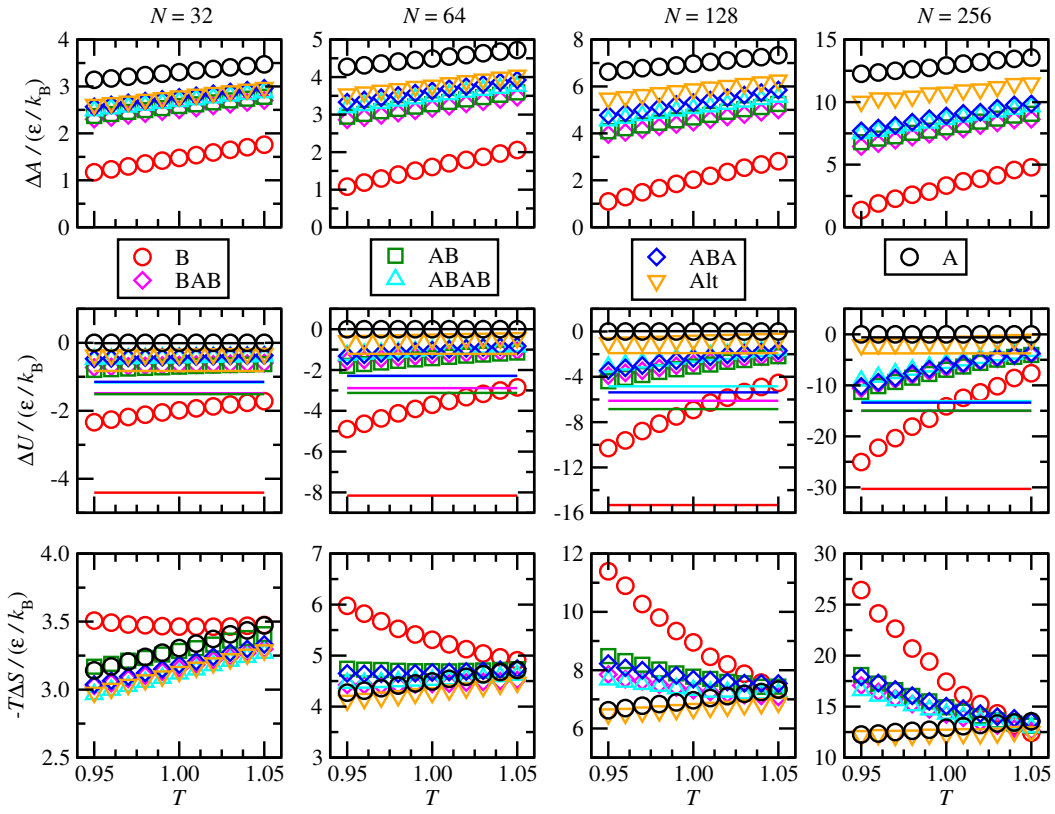

Figure 3.6: Helmholtz free energies, internal energies, and temperature– entropies of transfer for polymers partitioning into the spherical pore determined from Eq. 3.6. Solid lines designate values obtained from Eq. 3.5.

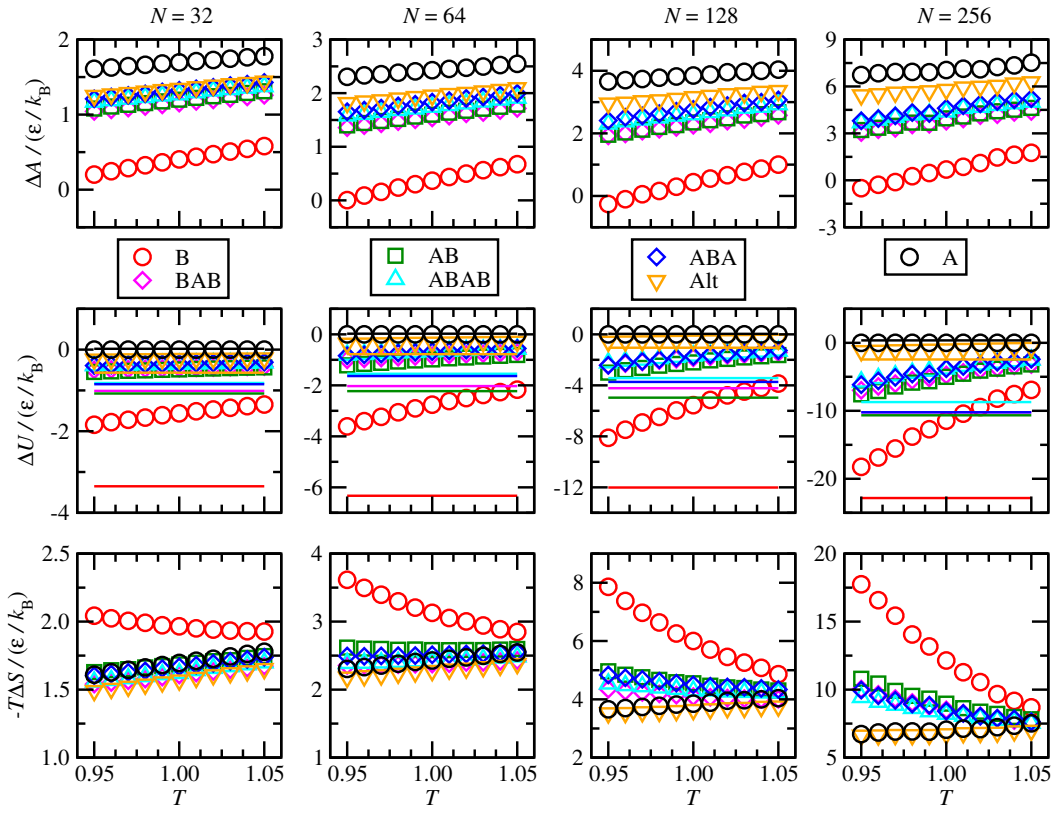

Figure 3.7: Helmholtz free energies, internal energies, and temperature– entropies of transfer for polymers partitioning into the cylindrical pore determined from Eq. 3.6. Solid lines designate values obtained from Eq. 3.5.

To confirm the results seen in Figures 3.6 and 3.7, the heat capacities of transfer may be determined from either the internal energy or entropy transfer with Eq. 3.7 and Eq. 3.8 [63]:

$$\Delta C_{\mathrm{v}} = \frac{\Delta U_{\mathrm{trans}}(T_{\mathrm{f}}) - \Delta U_{\mathrm{trans}}(T_{\mathrm{o}})}{T_{\mathrm{f}} - T_{\mathrm{o}}} \tag{3.7}$$

$$\Delta C_{\mathrm{v}} = \frac{\Delta S_{\mathrm{trans}}(T_{\mathrm{f}}) - \Delta S_{\mathrm{trans}}(T_{\mathrm{o}})}{\ln(T_{\mathrm{f}}/T_{\mathrm{o}})} \tag{3.8}$$

Three temperature ranges were used to determine the heat capacities to capture temperature effects: $T_{\mathrm{o}} = 0.95$ and $T_{\mathrm{f}} = 1.05$, $T_{\mathrm{o}} = 0.95$ and $T_{\mathrm{f}} = 0.96$, and $T_{\mathrm{o}} = 1.04$ and $T_{\mathrm{f}} = 1.05$. These heat capacities are presented in Tables 3.10, 3.11, 3.12, and 3.13 for $N = 32$, 64, 128, and 256, respectively.

Table 3.10: Heat capacities of transfer for polymers with $N = 32$ from the solution phase to spherical (SP) and cylindrical (CY) pores determined from Eq. 3.7 and Eq. 3.8. Errors given are standard errors of the mean.

		$T_o = 0.95$, $T_f = 1.05$		$T_o = 0.95$, $T_f = 0.96$		$T_o = 1.04$, $T_f = 1.05$	
Polymer	Pore	Eq. 3.7	Eq. 3.8	Eq. 3.7	Eq. 3.8	Eq. 3.7	Eq. 3.8
B	SP	2.477_{7}	1.529_{9}	3.09_{10}	2.06_{12}	1.93_{5}	1.12_{8}
	CY	1.979_{9}	1.260_{13}	2.55_{12}	1.62_{15}	1.54_{6}	0.82_{11}
BAB	SP	0.510_{4}	0.182_{9}	0.65_{4}	0.47_{8}	0.50_{3}	0.05_{9}
	CY	0.332_{3}	0.115_{9}	0.39_{3}	0.20_{8}	0.27_{3}	0.04_{10}
AB	SP	0.677_{5}	0.360_{11}	0.83_{4}	0.49_{11}	0.50_{5}	0.18_{10}
	CY	0.451_{3}	0.205_{10}	0.53_{3}	0.13_{10}	0.37_{4}	0.12_{10}
ABAB	SP	0.323_{3}	0.033_{8}	0.40_{3}	-0.04_{10}	0.26_{2}	0.04_{9}
	CY	0.261_{4}	0.088_{11}	0.29_{3}	0.20_{9}	0.22_{3}	0.09_{12}
ABA	SP	0.390_{3}	0.095_{9}	0.47_{3}	0.17_{9}	0.30_{3}	-0.05_{10}
	CY	0.327_{3}	0.123_{9}	0.44_{4}	0.15_{8}	0.26_{3}	0.03_{9}
Alter.	SP	0.197_{19}	0.006_{6}	0.24_{2}	0.08_{7}	0.175_{15}	-0.01_{7}
	CY	0.115_{19}	-0.015_{8}	0.13_{2}	-0.01_{10}	0.087_{18}	-0.04_{8}
A	SP	0	0.000_{13}	0	0.17_{8}	0	-0.12_{14}
	CY	0	0.004_{7}	0	0.00_{7}	0	0.05_{8}

Table 3.11: Heat capacities of transfer for polymers with $N = 64$ from the solution phase to spherical (SP) and cylindrical (CY) pores determined from Eq. 3.7 and Eq. 3.8. Errors given are standard errors of the mean.

		$T_o = 0.95$, $T_f = 1.05$		$T_o = 0.95$, $T_f = 0.96$		$T_o = 1.04$, $T_f = 1.05$	
Polymer	Pore	Eq. 3.7	Eq. 3.8	Eq. 3.7	Eq. 3.8	Eq. 3.7	Eq. 3.8
B	SP	8.18_3	6.46_4	10.4_3	8.60_4	6.1_2	4.2_3
	CY	5.75_3	4.37_4	8.2_3	6.26_4	3.8_2	2.7_4
BAB	SP	2.032_{13}	1.41_3	2.34_{12}	1.87_2	1.62_{11}	0.8_2
	CY	1.154_{15}	0.67_3	1.40_{17}	0.86_3	1.00_6	0.37_{16}
AB	SP	2.607_{15}	1.93_2	3.48_{19}	2.65_2	1.94_{14}	1.2_2
	CY	1.630_{12}	1.126_{17}	2.37_{13}	1.67_2	1.28_{13}	0.7_2
ABAB	SP	1.685_8	1.19_2	2.23_{10}	1.79_2	1.29_{10}	0.7_3
	CY	0.947_8	0.595_{18}	1.10_8	0.90_{16}	0.74_7	0.29_{16}
ABA	SP	1.988_{18}	1.51_2	2.6_2	2.24_3	1.48_{11}	1.0_2
	CY	1.139_{11}	0.78_2	1.42_{11}	1.228_{18}	0.87_{11}	0.5_2
Alter.	SP	0.594_5	0.31_3	0.65_6	0.27_3	0.53_3	0.2_3
	CY	0.307_4	0.111_{18}	0.36_3	0.09_2	0.25_4	-0.14_{17}
A	SP	0	0.02_2	0	0.23_{19}	0	0.2_2
	CY	0	0.006_{19}	0	-0.08_{16}	0	0.1_2

Table 3.12: Heat capacities of transfer for polymers with $N = 128$ from the solution phase to spherical (SP) and cylindrical (CY) pores determined from Eq. 3.7 and Eq. 3.8. Errors given are standard errors of the mean.

		$T_o = 0.95$, $T_f = 1.05$		$T_o = 0.95$, $T_f = 0.96$		$T_o = 1.04$, $T_f = 1.05$	
Polymer	Pore	Eq. 3.7	Eq. 3.8	Eq. 3.7	Eq. 3.8	Eq. 3.7	Eq. 3.8
B	SP	23.0_{2}	19.9_{2}	$27.1_{1.9}$	$24.5_{1.9}$	$14.4_{1.5}$	$11.7_{1.6}$
	CY	17.03_{15}	14.57_{17}	25_{2}	23_{2}	$13.8_{1.1}$	$10.7_{1.4}$
BAB	SP	7.27_{3}	6.07_{6}	10.0_{7}	9.6_{8}	5.2_{4}	4.1_{7}
	CY	4.00_{5}	3.04_{8}	5.3_{4}	4.6_{7}	3.0_{4}	1.6_{7}
AB	SP	8.84_{6}	7.38_{9}	12.0_{8}	10.3_{9}	5.0_{6}	2.6_{9}
	CY	5.51_{8}	4.488_{11}	7.6_{9}	$6.7_{1.2}$	3.7_{5}	3.0_{8}
ABAB	SP	5.89_{5}	4.85_{7}	7.5_{7}	6.3_{9}	3.4_{5}	2.1_{7}
	CY	3.69_{3}	2.981_{7}	5.0_{4}	4.1_{6}	3.1_{3}	1.6_{8}
ABA	SP	7.02_{7}	5.89_{9}	9.5_{8}	9.0_{9}	4.6_{8}	$3.2_{1.0}$
	CY	4.63_{9}	3.83_{11}	$7.9_{1.1}$	$5.8_{1.3}$	4.3_{5}	3.1_{7}
Alter.	SP	1.505_{15}	1.10_{5}	1.85_{19}	2.1_{4}	1.26_{13}	0.8_{5}
	CY	0.670_{11}	0.523_{4}	0.80_{15}	1.1_{6}	0.55_{11}	0.9_{7}
A	SP	0	-0.04_{4}	0	-0.3_{4}	0	-0.5_{5}
	CY	0	0.02_{9}	0	-0.2_{7}	0	0.0_{9}

Table 3.13: Heat capacities of transfer for polymers with $N = 256$ from the solution phase to spherical (SP) and cylindrical (CY) pores determined from Eq. 3.7 and Eq. 3.8. Errors given are standard errors of the mean.

		$T_o = 0.95$, $T_f = 1.05$		$T_o = 0.95$, $T_f = 0.96$		$T_o = 1.04$, $T_f = 1.05$	
Polymer	Pore	Eq. 3.7	Eq. 3.8	Eq. 3.7	Eq. 3.8	Eq. 3.7	Eq. 3.8
B	SP	70_8	64_8	100_{90}	100_{90}	30_{60}	30_{60}
	CY	$45.3_{1.2}$	$41.6_{1.2}$	56_{14}	50_{10}	20_{10}	20_{10}
BAB	SP	26_3	24_3	30_{30}	30_{30}	10_{30}	10_{30}
	CY	15.2_4	13.3_5	23_5	20_5	7_3	7_4
AB	SP	29_3	26_4	50_{40}	40_{40}	10_{30}	10_{30}
	CY	17.5_6	15.6_6	19_7	18_8	11_4	10_5
ABAB	SP	23_3	20_3	30_{30}	30_{30}	20_{30}	20_{30}
	CY	12.8_4	11.0_5	20_5	17_5	9_3	7_4
ABA	SP	26_4	26_4	30_{50}	30_{50}	10_{40}	20_{40}
	CY	15.0_6	15.6_6	22_8	20_8	11_4	11_5
Alter.	SP	4.3_6	3.4_7	7_7	1_7	3_7	5_7
	CY	1.89_8	1.3_2	$2.1_{1.0}$	2_2	1.4_8	1_2
A	SP	0	0.0_2	0	$1.1_{1.9}$	0	0_2
	CY	0	-3_3	0	-1_2	0	-4_2

The two methods for calculating heat capacities agree for the different sequences, pores, and temperature ranges. While the error bars are large for the small temperature ranges, the cylindrical pore heat capacities show a statistically significant difference between the two temperature ranges. This, in combination with Figures 3.6 and 3.7, highlights the temperature dependence of the thermodynamic transfer properties for polymer chains partitioning into a pore and suggest exercising caution when using the van't Hoff equation to examine polymers partitioning between different phases.

3.3.4 Structural Properties

The order of partition constants can be partially explained by examining the radial density profiles of the beads within the pore seen in Figure 3.8 for the spherical and

cylindrical pores, for four different values of N used in this work. Both sets of calculations use 40 equal volume spherical or cylindrical shells with $r = 0\sigma$ representing the center of the pore and $r = 20\sigma$ representing the pore wall. Only the outermost 5σ are shown here for clarity.

Both pores show similar trends with respect to the ordering of the chain segments. The **A** type beads are concentrated in the center of the pore and display a stronger preference for the pore center as N increases, which demonstrates the entropic penalty for having a longer chain near a confined surface. Amongst the copolymers, **A** beads in the **BAB** triblock sequence have the lowest prevalence near the pore wall, followed by the diblock, tetrablock, **ABA** triblock, and alternating sequences. This matches the order of the partition constants seen in Figure 3.4. These distributions have a similar shape to those seen for athermal beads in copolymers in a wide slit pore seen by Jiang et al. [27] While their block copolymers are composed of 50 **A** beads and 100 **B** beads, the same **A** density order is seen near the wall.

In the **B** homopolymer and block copolymers, the **B** type beads show a relatively constant distribution throughout the pore with a slight peak at approximately $r = 19\sigma$, followed by a steep decline between 19 and 20 σ. This peak corresponds to the distance for the attractive square-well potential for the **B** type beads. This peak near the pore wall with a plateau at farther distances agrees with self-consistent-field calculations of diblock copolymers consisting of one adsorbing block and one athermal block near a single wall [64].

Amongst the copolymers, the diblock exhibits the tallest peak, followed by the **BAB** triblock, tetrablock, **ABA** triblock, and alternating sequences. This illustrates the ability of part of a terminal block to adsorb at the pore wall and overcome the entropic penalty near the wall better than portions of the central blocks. This is similar to the retention order, but doesn't match exactly. Hence, while molecular level insight can provide some insight into polymer retention, examining spatial distributions at the monomer level is needed.

The probability of **B** monomers to "adsorb" or be within 1 σ of the pore wall in the spherical and cylindrical pores for polymers with $N = 32$, 64, 128, or 256 as a function of monomer position within the chain are displayed in Figure 3.9. An index of one or N indicates either chain end while $N/2$ is the center of the chain. The probability values are dependent on pore geometry, but the trends are consistent

between the two pores.

The distribution for the **B** hompolymer is relatively constant, outside of slight increases for approximately four units within each chain end, independent of chain length. The increased probability near the chain ends corresponds to the decreased steric hindrance these beads experience when adsorbing to the pore wall. This allows the effects of intersections between **A** and **B** beads to be elucidated from the distributions for the different copolymer sequences. There is a slight chain length dependence for the central **B** bead adsorption probability as it varies by a factor of 1.2 for $N = 32$ and $N = 256$ due to the lack of a true critical condition, but this does not prevent the observation of **A**–**B** intersection effects.

To better structure this discussion, let us initially focus on the copolymers with $N = 256$ to illustrate long chain behavior. The diblock, **BAB** triblock, and tetrablock sequences all contain long terminal **B** segments which exhibit similar increased adsorption probabilities for beads near the chain end as those in the homopolymer. For monomer indices near the chain end, but outside of the region affected by the terminus, the probabilities are very similar to those of the **B** homopolymer until the monomer index is roughly 32 units away from an intersection. This suggests that, at least for sufficiently long terminal blocks, **B** beads far away from **A**–**B** intersections adsorb very similarly to those in the **B** homopolymer.

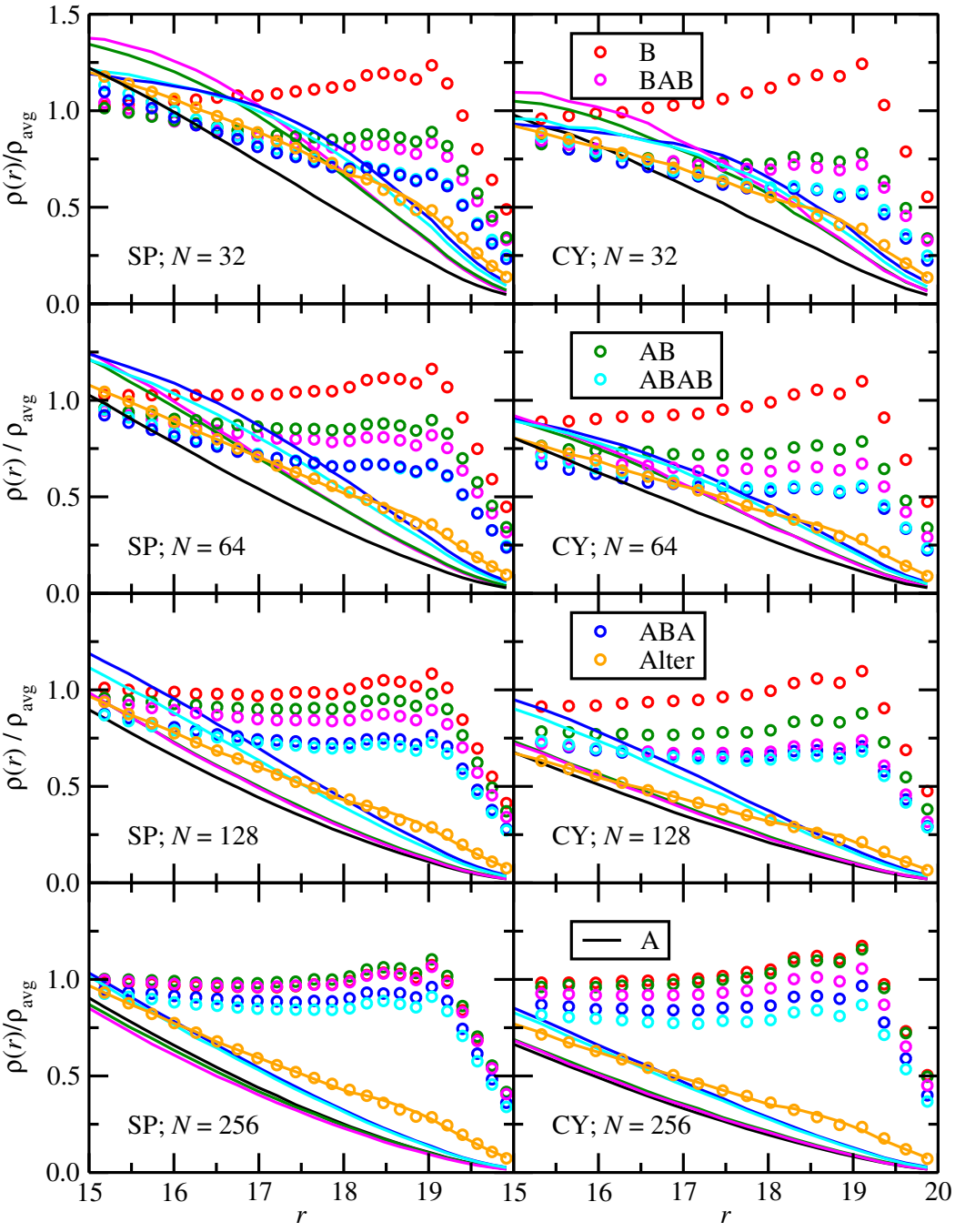

Figure 3.8: Normalized radial density profiles for polymers with $N = 32$ (top), $N = 64$ (second from top), $N = 128$ (second from bottom) and 256 (bottom) in the spherical (left) and cylindrical (right) pores. Symbols and lines denotes the data for the **B** and **A** segments, respectively.

The **ABA** triblock and tetrablock sequences both have **B** blocks within the middle of the chain, which allows for the effect of two nearby intersections on block adsorption probabilities. Beads near the intersection have a significantly decreased adsorption probability compared to the homopolymer beads at the same index. For indices near the center of the block, the adsorption probability approaches that of the **B** homopolymer. Those in the longer **ABA** triblock segment (index near $N/2$) agree with those in the homopolymer, while those in the shorter tetrablock segment (index near $3N/8$) have probabilities noticeably less than those in the homopolymer. This suggests that monomers in the middle of triblock segment aren't affected by the intersections while those in the tetrablock segment are still slightly affected; thus, an intersection does not affect adsorption for **B** beads far enough removed from it, and terminal **B** beads are not necessary for the beads to exhibit similar adsorption behavior as those in the homopolymer. Additionally, the **B** bead closest to an intersection has a very similar adsorption probability, independent of index and whether the sequence has two, three, or four blocks. This implies that the nearby intersection is the primary influence on the the adsorption probability, not monomer index.

In the alternating sequence, all **B** beads are neighboring an **A** bead and thus must overcome the unfavorable placement of an **A** bead near the pore wall to adsorb. This results in all beads having a much lower adsorption probability than those in the **B** homopolymer. There is still a significant increase for **B** monomers near the chain end compared to those in the middle of the chain, but they do not match those of corresponding **B** monomers in the **B** homopolymer due to the nearby **A** beads. For the central beads, the adsorption probabilities are less than those of the **B** beads part of an **A**–**B** intersection in the other copolymers due to the influence of multiple intersections nearby.

The distributions for $N < 256$ exhibit similar trends as those seen for $N = 256$. Increased probabilities for **B** beads near the chain ends are seen over a similar range of roughly four beads. Similarly shaped curves are found for the **B** blocks near intersections, but mid-block probabilities do not quite match those of the **B** homopolymer due to the shorter block length such that all beads within the block are affected by the intersection. Both the long-range decrease in adsorption probability from **A**–**B** intersections and short-range increase in adsorption probability from **B** beads near the termini are used to guide the development of a new calibration equation

discussed in the next section.

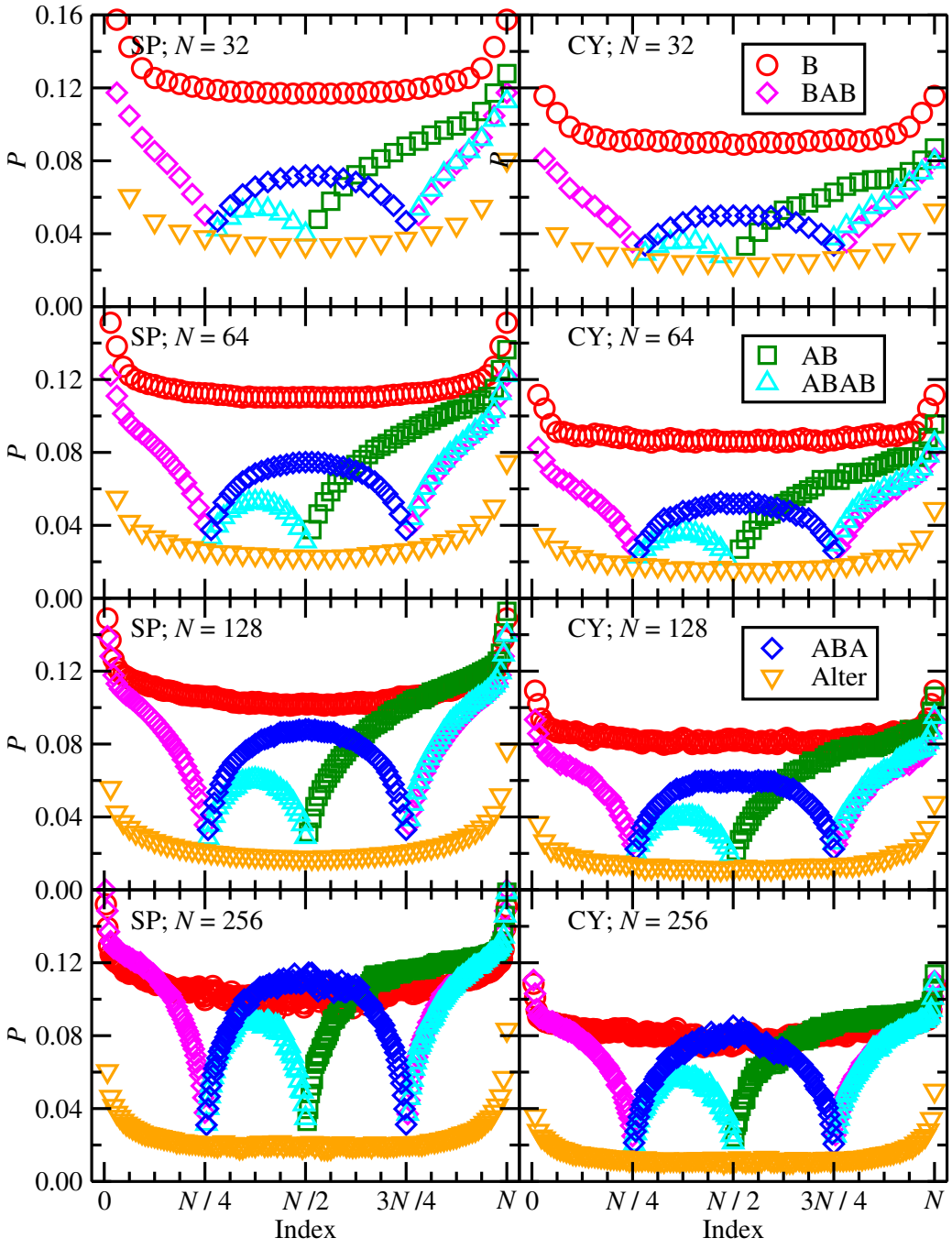

Figure 3.9: Probabilities for a favorable **B** segment–wall contact as function of segment index for polymers with $N = 32$, 64, 128, and 256 in the spherical and cylindrical pores.

The probability distributions for the **B** homopolymer, diblock, and **ABA** triblock are similar to those seen in a self-consistent-field theory study by Evers et al. [64] In their work, the **A** monomer is given a high affinity for a flat surface while the **B** monomers have the same affinity for the surface and the solvent. Both the **B** homopolymer distribution in this work and the **A** homopolymer distribution in their work are symmetric with enhanced adsorption near the chain ends. Their homopolymer data is for $N = 100$, but suggests a plateau in the adsorption probability for units in the middle of the chain. Both diblock and triblock distributions show an enhancement for interacting beads near the chain end, a plateau in adsorption probability for beads of intermediate distance from the chain end and/or **A**–**B** intersection and a significant decrease in adsorption probability near the intersection.

3.3.5 Sequence-Dependent Calibration Equation

Given the wide disparity between the the partition constants predicted by Eq. 3.4 and the actual partition constants seen in Figure 3.4, a new method to predict partition constants is clearly needed. There appears to be a lack of proposed equations that account for chain sequence to better predict polymer partition constants in the literature. In Figure 3.9, it is evident that the proximity to a chain end or an intersection with **A** beads increases or decreases the probability that a **B** bead adsorbs to the pore wall. When **B** beads are far enough removed from an intersection or a chain end, they have the same probability to adsorb as **B** beads within the middle of the **B** homopolymer. This sort of "saturation" behavior is analogous to Langmuir adsorption behavior. Adding terms to compensate for these observations to Eq. 3.4 leads to an equation with the form:

$$\begin{aligned} \ln K_{\mathrm{AB},N} = \ln K_{\mathrm{A},N/2} + \ln K_{\mathrm{B},N/2+1} - \ln K_{\mathrm{B},1} \\ + \frac{N_{\mathrm{i}} L_{\mathrm{block}}}{L_{\mathrm{block}} + C_1} \times C_2 + \frac{N_{\mathrm{t}} L_{\mathrm{block}}}{L_{\mathrm{block}} + C_3} \times C_4 \end{aligned} \tag{3.9}$$

where N_{i} is number of intersections between **A** and **B** beads, N_{t} is the number of **B** termini, L_{block} is the **B** block length in the copolymer, and C_1, C_2, C_3, and C_4 are constants fit to each pore shape (provided in Table 3.14). These constants were fit concurrently by using the "fminsearch" function within MATLAB [65] to minimize the sum of the errors squared for all five copolymer sequences at all four lengths.

Pore	C_1	C_2	C_3	C_4
Spherical	25.0	-0.256	6.25	0.153
Cylindrical	25.9	-0.176	10.1	0.103

Table 3.14: Fitted constants for new calibration curve, Eq. 3.9, for spherical and cylindrical pores.

Several sets of initial guesses for the constants were used to confirm that a global minimum was found. Closer examination of Figure 3.9 shows that an intersection decreases the adsorption probability for all beads within roughly 32 beads of it, so values near 26 are reasonable for C_1 while C_2 must be less than zero, given that the number of intersections decreases adsorption probability. Figure 3.9 shows that a **B** terminus increases the adsorption probability for only a few beads near the end, thus $C_3 < 10$ is reasonable, and C_4 must be greater than zero, given that these termini increase adsorption probability.

The differences between partition constants predicted by Eq. 3.4 or Eq. 3.9 and those calculated directly from simulation are presented in Figure 3.10 with the mean signed and mean unsigned errors presented in Table 3.15. Using these equations that account for decreased adsorption caused by intersections and increased adsorption for **B** located very close to the chain ends allows one to predict copolymer partition constants with very high accuracy. While the sets of constants are similar for the two pore shapes, the differences between them show that these values would need to be fitted for a specific column and solvent system used in a LCCC experiment.

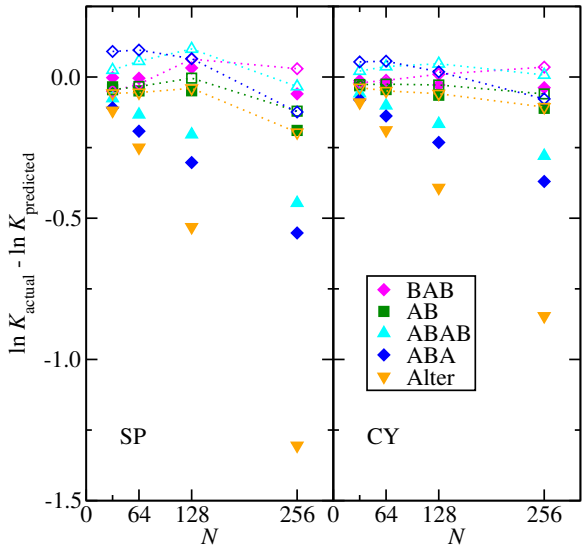

Figure 3.10: Errors in the logarithm of the partition constant for partition constants predicted by Eq. 3.4 (solid symbols) and by Eq. 3.9 (open symbols with dashed lines) in the spherical (left) and cylindrical (right) pores.

Reversing Equations 3.4 or 3.9 allows them to be used as calibration curves to determine the number of **A** beads in a chain, N_A. The partition constants from simulation are used to calculate the total length of the chain, which is then halved to yield N_A based on the knowledge that each chain is 50% of each monomer. Eq. 3.4 yields quite inaccurate N_A values, particularly at longer chain lengths and for the tetrablock, **ABA** triblock, and alternating sequences. This result questions the accuracy of large molecular weights determined from LCCC that use sequence-blind calibration curves. The new sequence-dependent equation has much lower errors in N_A for all sequences, at all lengths, and in both pores. Unlike the sequence-blind calibration equation, no one sequence has a significantly larger error than the other sequences when the new calibration equation is used. This shows that with general structural and composition information, molecular weights with less than 12% error can be determined from LCCC for many linear copolymer sequences.

	ln K				$N_{\mathrm{A,LCCC}}$			
	MSE		MUE		MSPE		MUPE	
	SP	CY	SP	CY	SP	CY	SP	CY
Eq. 3.3	-0.76	0.49	0.76	0.49	50	-8.5	54	19
Eq. 3.4	-0.24	-0.16	0.24	0.16	-27	-38	28	38
Eq. 3.9	-0.02	-0.01	0.07	0.04	-4.8	-6.7	11	11

Table 3.15: Mean signed (MSE) and unsigned (MUE) errors in the logarithm of the partition constants predicted by Equations 3.3, 3.4 and 3.9. Mean signed percentage (MSPE) and mean unsigned percentage (MUPE) errors in $N_{\mathrm{A,LCCC}}$ determined from Eq. 3.3, 3.4 and 3.9. "SP" and "CY" correspond to spherical and cylindrical pores, respectively.

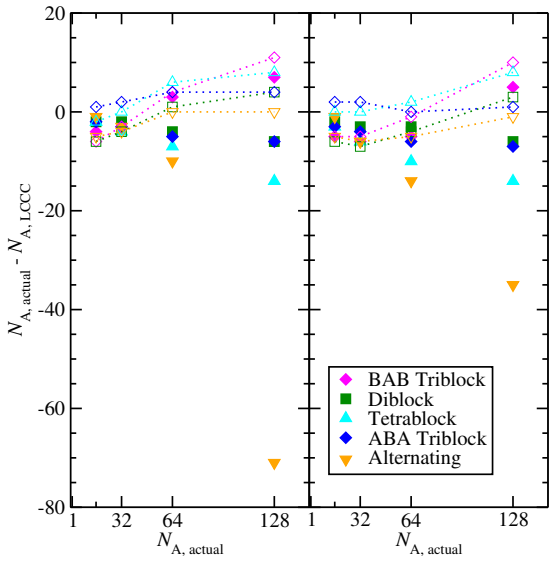

Figure 3.11: Error in N_{A} determined by using Eq. 3.4 (solid symbols) and Eq. 3.9 (open symbols with dotted lines) as calibration curves in the spherical (left) and cylindrical (right) pores.

3.4 Conclusions

In summary, we have presented a refined empirical model for the retention of block copolymers in LCCC based upon Gibbs ensemble Monte Carlo simulations. Partitioning between a mobile phase and a spherical or cylindrical pore was examined for five different copolymer sequences.

With the selected set of sequences, it was shown that monomer sequence does affect retention in LCCC, in agreement with experimental and simulation studies. [9, 54, 27]

Sequences with terminal **B** blocks are more retained than those with central **B** blocks. Spatial distributions of the monomers were used to guide the design of new calibration equations that account for both the number of **A**–**B** intersections and the number of **B** termini in a sequence. These new calibration curves decrease the the unsigned error in predicted partition constants and number of **A** segments determined by LCCC by a factor of four and a factor of ten for signed errors. This type of calibration equation has potential to accurately determine chain length for block copolymers though it does require more standards to fit.

References

[1] Sperling, L. Introduction to Physical Polymer Science. Wiley **2015**.

[2] Hiemenz, P. and Lodge, T. Polymer Chemistry, Second Edition. CRC Press **2007**.

[3] Bates, F. S., Hillmyer, M. A., Lodge, T. P., Bates, C. M., Delaney, K. T., and Fredrickson, G. H. Multiblock Polymers: Panacea or Pandora's Box? *Science 336* **2012**, 434–40.

[4] Pasch, H. and Trathnigg, B. HPLC of Polymers. Springer Science & Business Media **1999**.

[5] Striegel, A., Yau, W. W., Kirkland, J. J., and Bly, D. D. Modern Size-exclusion Liquid Chromatography: Practice of Gel Permeation and Gel Filtration Chromatography. John Wiley & Sons **2009**.

[6] Pasch, H. Liquid Chromatography at the Critical Point of Adsorption - A New Technique for Polymer Characterization. *Macromol. Symp. 110* **1996**, 107–120.

[7] Falkenhagen, J., Much, H., Stauf, W., and Muller, A. Characterization of Di-and Triblock Copolymers Using Coupled Chromatographic Methods. *Polym. Prepr. (Am. Chem. Soc.; Div. Polym. Chem.) 40* **1999**, 984–985.

[8] Falkenhagen, J., Much, H., Stauf, W., and Muller, A. H. E. Characterization of Block Copolymers by Liquid Adsorption Chromatography at Critical Conditions. 1. Diblock Copolymers. *Macromolecules 33* **2000**, 3687–3693.

[9] Park, I., Park, S., Cho, D. Y., Chang, T. Y., Kim, E., Lee, K. Y., and Kim, Y. J. Effect of Block Copolymer Chain Architecture on Chromatographic Retention. *Macromolecules 36* **2003**, 8539–8543.

[10] Biela, T., Duda, A., Rode, K., and Pasch, H. Characterization of Star-Shaped Poly(L-lactide)s by Liquid Chromatography at Critical Conditions. *Polymer 44* **2003**, 1851–1860.

[11] Vakhrushev, A. V., Gorbunov, A. A., Tezuka, Y., Tsuchitani, A., and Oike, H. Liquid Chromatography of Theta-Shaped and Three-Armed Star Poly(tetrahydrofuran)s: Theory and Experimental Evidence of Topological Separation. *Anal. Chem. 80* **2008**, 8153–8162.

[12] Neue, U. D. HPLC Columns: Theory, Technology, and Practice. Wiley **1997**.

[13] Braithwaite, A. and Smith, F. Chromatographic Methods. Kluwer Academic Publishers **1999**.

[14] Skoog, D. A., Holler, F. J., and Crouch, S. R. Principles of Instrumental Analysis, 6th Ed. Thomson Brooks/Cole **2007**.

[15] Ben-Naim, A. Statistical Thermodynamics for Chemists and Biochemists. Springer Science & Business Media **1992**.

[16] Martin, M. G. and Siepmann, J. I. Calculating Gibbs Free Energies of Transfer From Gibbs Ensemble Monte Carlo Simulations. *Theoretical Chemistry Accounts: Theory, Computation, and Modeling (Theoretica Chimica Acta) 99* **1998**, 347–350.

[17] Moore, J. Gel Permeation Chromatography. I. A New Method for Molecular Weight Distribution of High Polymers. *J. Polym. Sci. Part A: General Papers 2* **1964**, 835–843.

[18] Berek, D. Size Exclusion Chromatography–a Blessing and a Curse of Science and Technology of Synthetic Polymers. *J. Sep. Sci. 33* **2010**, 315–35.

[19] Li, Z. B., Kesselman, E., Talmon, Y., Hillmyer, M. A., and Lodge, T. P. Multicompartment Micelles from ABC Miktoarm Stars in Water. *Science 306* **2004**, 98–101.

[20] Moughton, A. O., Hillmyer, M. A., and Lodge, T. P. Multicompartment Block Polymer Micelles. *Macromolecules 45* **2012**, 2–19.

[21] Entelis, S. G., Evreinov, V. V., and Gorshkov, A. V. Functionality and Molecular Weight Distribution of Telechelic Polymers. In Pharmacy/Thermomechanics/Elastomers/Telechelics. Springer **1986**, 129–175.

[22] Olesik, S. V. Liquid Chromatography at the Critical Condition. *Anal. Bioanal. Chem. 378* **2004**, 43–45.

[23] Cifra, P. and Bleha, T. Steric Exclusion/Adsorption Compensation in Partitioning of Polymers into Micropores in Good Solvents. *Polymer 41* **2000**, 1003–1009.

[24] Cifra, P. and Bleha, T. Partition Coefficients and the Free Energy of Confinement from Simulations of Nonideal Polymer Systems. *Macromolecules 34* **2001**, 605–613.

[25] Gong, Y. C. and Wang, Y. M. Partitioning of Polymers into Pores Near the Critical Adsorption Point. *Macromolecules 35* **2002**, 7492–7498.

[26] Orelli, S., Jiang, W. H., and Wang, Y. M. A Computational Investigation of the Critical Condition Used in the Liquid Chromatography of Polymers. *Macromolecules 37* **2004**, 10073–10078.

[27] Jiang, W. H., Khan, S., and Wang, Y. M. Retention Behaviors of Block Copolymers in Liquid Chromatography at the Critical Condition. *Macromolecules 38* **2005**, 7514–7520.

[28] Ziebarth, J., Orelli, S., and Wang, Y. M. The Adsorption and Partitioning of Self-avoiding Walk Polymer Chains into Pores from a Bulk Theta Solution. *Polymer 46* **2005**, 10450–10456.

[29] Zhu, Y., Ziebarth, J. D., Macko, T., and Wang, Y. M. How Well Can One Separate Copolymers According to Both Chemical Compositions and Sequence Distributions? *Macromolecules 43* **2010**, 5888–5895.

[30] Yang, X., Zhu, X., and Wang, Y. M. Can the Individual Block in Block Copolymer be Made Chromatographically "Invisible" at the Critical Condition of its Corresponding Homopolymer? *Polymer 54* **2013**, 3730–3736.

[31] McQuarrie, D. Statistical Mechanics. University Science Books **2000**.

[32] Hill, T. L. An Introduction to Statistical Thermodynamics. Dover Publications, Inc, New York **1986**.

[33] Sugita, Y. and Okamoto, Y. Replica-exchange Molecular Dynamics Method for Protein Folding. *Chem. Phys. Lett. 314* **1999**, 141–151.

[34] Laio, A. and Parrinello, M. Escaping free-energy Minima. *Proc. Natl. Acad. Sci. 99* **2002**, 12562–12566.

[35] Metropolis, N., Rosenbluth, A. W., Rosenbluth, M. N., Teller, A. H., and Teller, E. Equation of State Calculations by Fast Computing Machines. *J. Chem. Phys. 21* **1953**, 1087–1092.

[36] Allen, D. J., M. P.; Tildesley. Computer Simulation of Liquids. Oxford Science Publ. Clarendon Press **1989**.

[37] Panagiotopoulos, A. Z. Direct Determination of Phase Coexistence Properties of Fluids by Monte Carlo Simulation in a New Ensemble. *Mol. Phys. 61* **1987**, 813–826.

[38] Panagiotopoulos, A. Z., Quirke, N., Stapleton, M., and Tildesley, D. J. Phase-Equilibria by Simulation in the Gibbs Ensemble - Alternative Derivation, Generalization and Application to Mixture and Membrane Equilibria. *Mol. Phys. 63* **1988**, 527–545.

[39] Frenkel, D. and Smit, B. Understanding Molecular Simulation: from Algorithms to Applications, vol. 1. Elsevier (formerly published by Academic Press) **2002**.

[40] Rosenbluth, M. N. and Rosenbluth, A. W. Monte Carlo Calculation of the Average Extension of Molecular Chains. *J. Chem. Phys. 23* **1955**, 356–359.

[41] Siepmann, J. I. A Method for the Direct Calculation of Chemical-potentials for Dense Chain Systems. *Mol. Phys. 70* **1990**, 1145–1158.

[42] Siepmann, J. I. and Frenkel, D. Configurational Bias Monte Carlo: A New Sampling Scheme for Flexible Chains. *Mol. Phys. 75* **1992**, 59–70.

[43] Frenkel, D., Mooij, G. C. A. M., and Smit, B. Novel Scheme to Study Structural and Thermal-properties of Continuously Deformable Molecules. *J. Phys.: Condes. Matter 4* **1992**, 3053–3076.

[44] De Pablo, J., Laso, M., and Suter, U. W. Estimation of the Chemical-potential of Chain Molecules by Simulation. *J. Chem. Phys. 96* **1992**, 6157–6162.

[45] Vlugt, T. J. H., Martin, M. G., Smit, B., Siepmann, J. I., and Krishna, R. Improving the Efficiency of the Configurational-bias Monte Carlo Algorithm. *Mol. Phys. 94* **1998**, 727–733.

[46] Martin, M. G. and Siepmann, J. I. Novel Configurational-bias Monte Carlo Method for Branched Molecules. Transferable Potentials for Phase Equilibria. 2. United-atom Description of Branched Alkanes. *J. Phys. Chem. B 103* **1999**, 4508–4517.

[47] Vlugt, T. J. H., Krishna, R., and Smit, B. Molecular Simulations of Adsorption Isotherms for Linear and Branched Alkanes and Their Mixtures in Silicalite. *J. Phys. Chem. B 103* **1999**, 1102–1118.

[48] Sun, T., Chance, R. R., Graessley, W. W., and Lohse, D. J. A Study of the Separation Principle in Size Exclusion Chromatography. *Macromolecules 37* **2004**, 4304–4312.

[49] Wang, Y., Teraoka, I., Hansen, F. Y., Peters, G. H., and Hassager, O. A Theoretical Study of the Separation Principle in Size Exclusion Chromatography. *Macromolecules 43* **2010**, 1651–1659.

[50] Casassa, E. F. and Tagami, Y. An Equilibrium Theory for Exclusion Chromatography of Branched and Linear Polymer Chains. *Macromolecules 2* **1969**, 14–26.

[51] Casassa, E. F. Comments on Exclusion of Polymer-Chains From Small Pores and its Relation to Gel-Permeation Chromatography. *Macromolecules 9* **1976**, 182–185.

[52] Casassa, E. F. Confined Random-Flight Polymer-Chains in Solution - Exclusion from Micropores and Distribution Near Barriers. *J. Polym. Sci. Pol. Sym.* **1985**, 151–160.

[53] Lee, H. J., Chang, T. Y., Lee, D. S., Shim, M. S., Ji, H. N., Nonidez, W. K., and Mays, J. W. Characterization of Poly(L-lactide)-block-poly(ethylene oxide)-block-poly(L-lactide) Triblock Copolymer by Liquid Chromatography at the Critical Condition and by MALDI-TOF Mass Spectrometry. *Anal. Chem. 73* **2001**, 1726–1732.

[54] Cho, D., Noro, A., Takano, A., and Matsushita, Y. TGIC Separation of PS-b-P2VP Diblock and P2VP-b-PS-b-P2VP Triblock Copolymers According to Chemical Composition. *Macromolecules 38* **2005**, 3033–3036.

[55] Zhu, Y., Ziebarth, J. D., and Wang, Y. M. Dependence of Critical Condition in Liquid Chromatography on the Pore Size of Column Substrates. *Polymer 52* **2011**, 3219–3225.

[56] Bai, J. I., P.; Siepmann. Selective Adsorption from Dilute Solutions: Gibbs Ensemble Monte Carlo Simulations. *Fluid Phase Equilib. 351* **2013**, 1–6.

[57] Lindsey, R. K., Rafferty, J. L., Eggimann, B. L., Siepmann, J. I., and Schure, M. R. Molecular Simulation Studies of Reversed-phase Liquid Chromatography. *J. Chromatogr. A 1287* **2013**, 60–82.

[58] Mooij, G. C. A. M., Frenkel, D., and Smit, B. Direct Simulation of Phase Equilibria of Chain Molecules. *J. Phys.: Condes. Matter 4* **1992**, L255.

[59] de Pablo, J. J., Laso, M., Siepmann, J. I., and Suter, U. W. Continuum-Configurational-Bias Monte Carlo Simulations of Long-Chain Alkanes. *Mol. Phys. 80* **1993**, 55–63.

[60] De Gennes, P.-G. Scaling Concepts in Polymer Physics. Cornell University Press **1979**.

[61] Rafferty, J. L., Siepmann, J. I., and Schure, M. R. Advances in Chromatography, vol. 48, chap. Understanding the Retention Mechanism in Reversed-Phase Liquid

Chromatography: Insights from Molecular Simulation. CRC Press: Boca Raton, FL **2010**, 10–55.

[62] Ziebarth, J. D. and Wang, Y. M. Interactions of Complex Polymers with Nanoporous Substrate. *Soft Matter 12* **2016**, 5245–5256.

[63] Wick, C. D., Siepmann, J. I., and Schure, M. R. Temperature Dependence of Transfer Properties: Importance of Heat Capacity Effects. *J. Phys. Chem. B 107* **2003**, 10623–10627.

[64] Evers, O. A., Scheutjens, J. M. H. M., and Fleer, G. J. Statistical Thermodynamics of Block Copolymer Adsorption. 1. Formulation of the Model and Results for the Adsorbed Layer Structure. *Macromolecules 23* **1990**, 5221–5233.

[65] The MathWorks Inc., Natick, MA. MATLAB and Statistics Toolbox, 2015a ed. **2015**.

Appendix A

Acronyms

Table A.1: Acronyms used in the present work.

CBMC	Configurational-bias Monte Carlo
GEMC	Gibbs ensemble Monte Carlo
MWD	Molecular weight distribution
LC	Liquid chromatography
LCCC	Liquid chromatography at the critical condition
MC	Monte Carlo
SEC	Size exclusion chromatography